Trehalose-6-phosphate links singlet oxygen-induced signalling with metabolic signalling in *Chlamydomonas reinhardtii*

Waeil Al Youssef[1], Regina Feil[2], Maureen Saint-Sorny[3], Xenie Johnson[3], John E. Lunn[2], Bernhard Grimm[1], and Pawel Brzezowski[1*]

Affiliation:

[1]Humboldt-Universität zu Berlin, Institut für Biologie/Pflanzenphysiologie, 10115 Berlin, Germany

[2]Max Planck Institute of Molecular Plant Physiology, 14476 Potsdam-Golm, Germany

[3]Aix Marseille Université, CNRS, CEA, Institut de Biosciences et Biotechnologies Aix-Marseille, Photosynthesis and Environment team, CEA Cadarache, 13108 Saint-Paul-lez-Durance, France.

*e-mail: pawel.brzezowski@hu-berlin.de

Abstract

Singlet oxygen ($^1O_2$) induces retrograde signalling in chloroplasts. Using a novel mutant screen, we identified a mutation in the *TREHALOSE-6-PHOSPHATE PHOSPHATASE 1* (*T6PP1*) gene that results in accumulation of trehalose 6-phosphate, a reprogramming of cell metabolism, and impairment of $^1O_2$-induced retrograde signalling in *Chlamydomonas reinhardtii*. From transcriptomic analysis and metabolite profiling, we conclude that accumulation or deficiency of certain metabolites directly affect $^1O_2$-signalling. $^1O_2$-inducible *GLUTATHIONE PEROXIDASE 5* (*GPX5*) gene expression is suppressed by increased content of fumarate, an intermediate in the tricarboxylic acid cycle (TCA cycle) in mitochondria and dicarboxylate metabolism in the cytosol, while it is promoted by another TCA cycle intermediate, aconitate. Furthermore, genes encoding known essential components of chloroplast-to-nucleus $^1O_2$-signalling show decreased transcript levels in a *t6pp1* mutant, which can be rescued by exogenous application of aconitate. We demonstrate that chloroplast retrograde signalling involving $^1O_2$ depends on mitochondrial and cytosolic processes and that the metabolic status of the cell determines the response to $^1O_2$.

35 **Introduction**

36 Nearly forty years ago, tetrapyrrole biosynthesis (TBS) intermediates were proposed to be
37 involved in chloroplast retrograde (organelle-to-nucleus) signalling. This conclusion was
38 based on the observation that accumulation of chlorophyll precursors negatively affects
39 transcript level of light-harvesting chlorophyll a/b-binding (LHCB) protein[1]. Later studies on
40 chloroplast retrograde signalling involved mutants[2], treatment with a carotenoid biosynthesis
41 inhibitor, norflurazon[3], or TBS inhibitors, such as α,α-dipyridyl [1] or thujaplicin[4]. Experiments
42 with norflurazon led to the discovery of the *genomes uncoupled* (*gun*) mutants with a
43 common phenotype of chloroplast status-independent expression of photosynthesis-
44 associated nuclear genes[3].

45 It is noteworthy that treatment with inhibitors causing carotenoid deficiencies results
46 in generation of reactive oxygen species (ROS) and photooxidative damage to chloroplasts.
47 Furthermore, the end-products of TBS, haem and chlorophyll, as well as many of their
48 intermediates (Supplementary Fig. 1) are light-absorbing and redox-reactive molecules,
49 capable to generate ROS. Singlet oxygen ($^1O_2$) can be produced through interaction of ground
50 (triplet)-state oxygen ($^3O_2$) with triplet-state chlorophyll or TBS intermediates, e.g.
51 protoporphyrin IX (Proto), which are excited by light[5]. ROS are also metabolic products of
52 other cellular processes in plants, such as photosynthesis and respiration.

53 Although $^1O_2$ is not considered to be the most reactive oxygen species, it is thought to
54 be the major ROS involved in photooxidative damage[6]. However, it was shown that
55 production of $^1O_2$ in the chloroplast induces stress responses that do not result exclusively
56 from physicochemical damage, but also rely on signal transduction triggered by ROS[7].
57 Additionally, studies on the *fluorescent* (*flu*) mutant of *Arabidopsis thaliana*, which is
58 impaired in regulation of TBS and accumulates protochlorophyllide (Supplementary Fig. 1),
59 demonstrated that $^1O_2$-retrograde signalling is integrated into a broader signalling network
60 and affects not only stress responses but also metabolism[8].

61 However, $^1O_2$ has a short half-life (about 200 ns) in the cell[9]. As a result, the distance
62 that it may move was calculated to be approximately 10 nm, based on predicted diffusion
63 rates[10,11]. Its diffusion range is also limited due to its high reactivity with membrane lipids.
64 Therefore, $^1O_2$ could play a specific role as an activator of a stress response only if it is
65 detected close to its source, which strongly suggests that other components mediating the $^1O_2$
66 signals should exist. Alternatively, altered metabolite contents triggered by $^1O_2$ may also
67 mediate $^1O_2$-retrograde signalling, or as proposed by Pfannschmidt [12], a certain metabolic
68 signature may be required to trigger changes in nuclear gene expression.

69 Despite the profound effect of $^1O_2$ on the chloroplast redox state and its apparent
70 involvement in altering nuclear gene expression, little is known about the components
71 involved in $^1O_2$-dependent retrograde signalling. The protein factors identified so far include
72 EXECUTER1 (EX1) and EX2 in the *flu* mutant of *A. thaliana*[13], PSBP DOMAIN-
73 CONTAINING PROTEIN 2 (PSBP2[14] and SINGLET OXYGEN ACCLIMATION (SAK1[15]
74 in *Chlamydomonas reinhardtii*, or METHYLENE BLUE SENSITIVITY (MBS1[16] shown to
75 be involved in $^1O_2$-signalling in both *A. thaliana* and *C. reinhardtii*.
76 In our search for tetrapyrrole-signalling components, we hypothesized that $^1O_2$
77 generated via the photosensitizing activity of Proto, rather than porphyrin accumulation itself,
78 triggers signalling cascades that alter nuclear gene expression. Therefore, we used a *C.*
79 *reinhardtii* mutant *chlD-1*[17] that accumulates Proto due to a dysfunctional Mg-chelatase
80 (MgCh, Supplementary Fig.1). The GENOMES UNCOUPLED 4 (GUN4) protein involved
81 in MgCh function (Supplementary Fig. 1) and signalling degrades upon Proto
82 accumulation[18]. However, *chlD-1* with introduced over-expression of GUN4, *chlD-1/GUN4*,
83 showed higher GUN4 content than *chlD-1*, but retained the chlorophyll-free phenotype[18].
84 Additionally, *chlD-1/GUN4* demonstrated higher expression of *GPX5* and higher tolerance to
85 $^1O_2$ than *chlD-1*[18]. Thus, to minimize the GUN4-deficient phenotype and to maintain high
86 and stable $^1O_2$-inducibility of *GPX5* expression, *chlD-1/GUN4* was used as a background
87 strain instead of *chlD-1* in the present study to monitor $^1O_2$-signalling. For this purpose,
88 expression of the *GLUTATHIONE PEROXIDASE 5* (*GPX5*) gene, which is specifically
89 induced by $^1O_2$ in *C. reinhardtii*[19,20] was used as a marker gene. The $^1O_2$-inducible promoter
90 region of *GPX5* fused to the promoterless *ARYLSULFATASE 2* gene (*ARS2*) was shown to be
91 an effective reporter to study *GPX5* expression[14,20,21].
92 Mutagenesis of the strain carrying the *GPX5-ARS2* reporter (in a *chlD-1/GUN4*
93 mutant background), followed by a screening for decreased reporter gene expression
94 identified a mutant impaired in $^1O_2$-signalling. The lack of the retrograde response to $^1O_2$ in
95 this mutant was verified to decrease expression of *GPX5*, as well as *SAK1*, *MBS*, and *PSBP2*.
96 The causal mutation was found in a gene annotated as *TREHALOSE 6-PHOSPHATE*
97 *PHOSPHATASE* (hereafter *T6PP1*). Besides clear impairment in $^1O_2$-signalling, mutation in
98 *T6PP1* also resulted in accumulation of trehalose 6-phosphate (Tre6P). Therefore, T6PP1 is
99 the first confirmed phosphatase acting on Tre6P in *C. reinhardtii* and in fact the first enzyme
100 with a confirmed function in trehalose metabolism in this organism. Our data indicate that
101 accumulation of Tre6P causes changes to the expression of genes involved in several
102 metabolic pathways. However, Tre6P is an intermediate rather than the primary cause of the

103 impaired $^1O_2$-signalling. Here using a combination of genetics, gene expression and
104 metabolic phenotypes, we reveal a complex interaction between chloroplast, mitochondria
105 and cytosol in $^1O_2$ signal transmission to the nucleus.
106
107 **Results**
108 **Forward genetics screen to identify components of the $^1O_2$-signalling**
109 To generate a mutant impaired in $^1O_2$-dependent signalling, we first created a reporter strain
110 in a known $^1O_2$-generating mutant, which was subsequently subjected to mutagenesis. The
111 *GPX5-ARS2* reporter construct (Supplementary Fig. 2) was introduced into the genome of
112 *chlD-1/GUN4* to express the ARS2 protein in a $^1O_2$-dependent manner, and the transformants
113 were tested for the enzymatic activity of ARS2. The reporter strain, which showed the lowest
114 ARS2 activity in darkness and the highest activity in light was named *signalling Reporter*
115 (*sigRep*; Fig. 1a) and was used in further applications. Expression kinetics of the cytosolic
116 ($GPX5_{cyt}$) and chloroplastic ($GPX5_{cp}$) version of *GPX5*[22]; Supplementary Fig. 2), as well as
117 the *GPX5-ARS2* construct were examined by quantitative Real-Time PCR (qRT-PCR) upon
118 transfer from dark to light. As expected, higher induction of $GPX5_{cp}$ and $GPX5_{cyt}$ were
119 observed upon light illumination in *sigRep* compared to WT (Fig. 1b). Induced *GPX5-ARS2*
120 expression in *sigRep* in the light (Fig. 1c) confirmed the results obtained in the ARS activity
121 assay (Fig. 1a).
122 Subsequently, a random mutagenesis was performed on *sigRep* using bleomycin
123 resistance cassette (ble^R) as an insert, followed by screening to isolate strains with lower or
124 undetectable ARS2 activity in the light compared to *sigRep*, and thus, possibly disrupted $^1O_2$-
125 dependent signalling. Screen of 804 transformants allowed us to isolate nine, which were
126 named *genomes uncoupled Singlet Oxygen Signalling* (*gunSOS*). The *gunSOS1* mutant (Fig.
127 1d) was selected for further analysis. Higher sensitivity to light was recorded in *gunSOS1*
128 compared to the *sigRep* background strain (Fig. 1e), in agreement with a higher sensitivity or
129 impaired acclimation to $^1O_2$. Mutant impaired in $^1O_2$-signalling showed similar Proto
130 accumulation in light compared to *sigRep* and *chlD-1/GUN4* (Supplementary Fig. 3), which
131 eliminated the possibility that spurious mutations in *gunSOS1* resulted in reduced content of
132 this photosensitizer.
133 The ble^R insertion in *gunSOS1* was located in the first exon of the gene annotated as
134 *TREHALOSE 6-PHOSPHATE PHOSPHATASE 1* (here *T6PP1*; locus Cre12.g497750) in the
135 JGI portal (Department of Energy Joint Genome Institute, https://phytozome-
136 next.jgi.doe.gov, v13, genome v5.6; Fig. 1f). The *T6PP1* transcript abundance was

137 determined in *gunSOS1* and compared to *sigRep* by qRT-PCR using primers annealing to the
138 coding sequence upstream of the insertion site. At 2 h after transfer from dark to light, *T6PP1*
139 mRNA content increased 2.5-fold in *sigRep* compared to WT, while it was virtually absent in
140 *gunSOS1* (Fig. 1g). Expression of $GPX5_{cyt}$ and $GPX5_{cp}$ was nearly 10 and 8 times lower in
141 *gunSOS1* compared to *sigRep*, respectively (Fig. 1h). The transcript abundance for *GPX5-*
142 *ARS2* was 7 times lower in *gunSOS1* than in *sigRep* (Fig. 1i), and explains undetectable
143 ARS2 activity in the $^1O_2$-signalling mutant (Fig. 1d).
144

145 ***C. reinhardtii* T6PP1 is a functional Tre6P phosphatase**

146 While *gunSOS1* is clearly impaired in $^1O_2$-signalling, it was necessary to determine the
147 primary phenotype caused by the mutation in *T6PP1*. The content of Tre6P in *sigRep* and
148 *gunSOS1* was determined by anion-exchange high performance liquid chromatography
149 coupled to tandem mass spectrometry (LC-MS/MS). Tre6P accumulation increased in
150 *gunSOS1* upon exposure to light in a time-dependent manner, while it decreased in *sigRep*
151 (Fig. 2a). Accumulation of Tre6P in *gunSOS1* indicates that *C. reinhardtii* T6PP1 is a
152 functional phosphatase dephosphorylating Tre6P to trehalose. Subsequently, *T6PP1*
153 expression was found to be induced in the light in *sigRep*, but not in the WT, indicating its
154 inducibility by photooxidative stress rather than light (Fig. 2b). Mutation of the *T6PP1* gene
155 would be expected to lower Tre6P phosphatase activity and dephosphorylation of Tre6P to
156 trehalose, but we also observed accumulation of trehalose in *gunSOS1* (Fig. 2c). This
157 apparent discrepancy can be explained by the existence of another enzyme in *C. reinhardtii*
158 with possible Tre6P phosphatase activity, in combination with higher levels of Tre6P (see
159 Discussion section).

160 Rescue of the T6PP1 deficiency in *gunSOS1* was performed with the isolated genomic
161 DNA fragment carrying the wild-type *T6PP1* gene. Several independent transformants
162 showed rescued $^1O_2$-signalling, which was indicated by the *GPX5-ARS2* expression
163 determined in the ARS assay, and data from three representative strains are shown in
164 Supplementary Fig. 4a. The analysed rescued strains also showed increased $GPX5_{cp}$ transcript
165 content compared to *gunSOS1* (Supplementary Fig. 4b). A peptide-specific antibody for
166 T6PP1 was produced to compare the protein content in *gunSOS1* to strains showing $^1O_2$-
167 dependent signalling. A faint immune signal of approximately 43 kDa was detected in
168 *gunSOS1* and *chlD-1*, but two narrow bands were seen in *chlD-1/GUN4*, *sigRep* and the
169 *T6PP1*-rescued strains (Fig. 2d). WT and *gunSOS1* showed an additional unspecific
170 immunoreaction with protein of approximately 53 kDa. As expected, GPX5 content was

171 lower in *gunSOS1* compared to *sigRep* (Fig. 2d), which correlated with qRT-PCR results on
172 *GPX5* transcript levels (Fig. 1 h). Strains with rescued $^1O_2$-signalling, *T6PP1-R1, -R2, and -*
173 *R3*, showed increased content of GPX5 (Fig. 2d) and higher tolerance to light compared to
174 *gunSOS1* (Fig. 2e).
175
176 **The *gunSOS1* mutant shows altered metabolism compared to *sigRep***
177 In *A. thaliana* and other angiosperms, Tre6P functions as a sucrose signal and homeostatic
178 regulator of sucrose metabolism[23,24], which links plant growth and development to the
179 availability of sucrose[25], reviewed in[26]. To determine the effect of accumulated Tre6P on
180 metabolism in *C. reinhardtii*, we performed comparative metabolite profiling of *gunSOS1*
181 and *sigRep* (Supplementary Table 1), which revealed a relatively wide range of variation.
182 Aside from Tre6P and trehalose, 11 out of 27 analysed metabolites showed significantly
183 increased content in *gunSOS1* compared to *sigRep* in the light (Figure 3a). By means of the
184 MetaboAnalyst 5.0 portal (https://www.metaboanalyst.ca) these metabolites were assigned to
185 the metabolic processes in the cell. A hypergeometric test indicated the most affected
186 metabolic pathways, i.e. the TCA cycle, pyruvate metabolism, and starch and sucrose
187 metabolism (Fig. 3b, Supplementary Table 2). Eight metabolites showed significantly
188 decreased content in *gunSOS1* compared to *sigRep* (Fig. 4a), with the highest impact
189 (MetaboAnalyst 5.0) on fructose and mannose metabolism, amino sugar and nucleotide sugar
190 metabolism, and starch and sucrose metabolism (Fig. 4b, Supplementary Table 3).
191 Metabolites, which did not show a significant change in *gunSOS1* compared to *sigRep* are
192 presented in Supplementary Fig. 5.
193 Starch content was determined in *gunSOS1* and compared to *sigRep*, because of
194 changes in several intermediates of starch and sucrose metabolism (Fig. 3b and Fig. 4b).
195 Indeed, *gunSOS1* accumulated only 60% of the starch content of *sigRep* when the strains
196 were grown in acetate-supplemented media (TAP, Fig. 4c). Both *sigRep* and *gunSOS1* are
197 obligate heterotrophs. *SigRep* contained less starch after transfer from TAP and cultivation in
198 TP for 48 h, whereas the starch content of *gunSOS1* was essentially unchanged (Fig. 4c),
199 indicating that there was net degradation of starch in *sigRep* but not in *gunSOS1*.Starch
200 formation is strongly induced during nitrogen (N) deprivation[27]. The *sigRep* cells did not
201 increase starch reserves after 3 days in N-deficient medium, suggesting that starch
202 accumulation had already reached its maximum under non-stress conditions. The starch
203 content in *gunSOS1* deprived of N did increase by 50% and was similar to the content in
204 *sigRep* (Fig. 4c). We conclude that *sigRep* accumulates high levels of starch as a

205 consequence of the *chlD-1/GUN4* genetic background and that the accumulation of Tre6P
206 represses this response in *gunSOS1* leading to a lower accumulation of starch. The *gunSOS1*
207 cells are still capable of responding to the N-deprivation stress and accumulating starch
208 despite disturbed metabolism. Starch degradation on the other hand, is compromised in
209 *gunSOS1*, which could indicate a general impairment of catabolic processes or a defect in
210 sensing carbon limitation. The map-overview of the selected metabolic pathways with
211 depicted metabolites that showed different content, or were not changed, in *gunSOS1* relative
212 to *sigRep* is presented in Figure 5.
213

214 **Increased Tre6P content alters metabolism in *C. reinhardtii* via alteration of the**
215 **transcriptome**

216 To determine the extent to which chloroplast retrograde signalling is affected in *gunSOS1*, we
217 performed comparative RNA-sequencing (RNA-seq) of the transcriptomes of *gunSOS1* and
218 *sigRep* upon transfer from dark to light. The analysis showed that 8120 genes were expressed
219 in both strains, but 1377 and 1087 additional genes were uniquely expressed in *gunSOS1* and
220 *sigRep*, respectively (Fig. 6a, detailed listing can be found in Supplementary Data Set 1).
221 Furthermore, differential gene expression analysis showed that the transcript contents of 1606
222 genes and 1706 genes were lower or higher, respectively, in *gunSOS1* compared to *sigRep*
223 (Supplementary Data Set 2).

224 Based on the KEGG ontology (http://www.kegg.jp/) several genes associated with
225 metabolic pathways were down- (Fig. 6b) or up-regulated (Fig. 6c) in *gunSOS1* compared to
226 *sigRep* (Supplementary Data Set 3). Given the strong overlap between differentially
227 expressed genes and corresponding pathway intermediates, we hypothesized that the altered
228 metabolism can be directly explained by altered gene expression. To decipher a complex
229 correlation between altered signalling, gene expression and metabolism, accumulation or
230 deficiency in metabolites from given pathway(s) was correlated with altered gene expression
231 in *gunSOS1* compared to *sigRep*. Fumarate and aconitate will be described in more detail, as
232 representative examples of the metabolites showing respectively increased or decreased
233 content in *gunSOS1* compared to *sigRep*.

234 KEGG enrichment of the RNA-seq data indicated increased expression of the gene
235 encoding FUMARATE HYDRATASE CLASS II (FUM2, Enzyme Commission (EC)
236 Number 4.2.1.2, Cre01.g020223) in *gunSOS1* compared to *sigRep*. FUM is responsible for
237 reversible stereospecific interconversion of malate to fumarate. However, specific isoforms of
238 this protein act in defined pathways and may favour one direction over the other depending

239 on the subcellular localisation and environment[28]. The mitochondrial isoform catalyses
240 hydration of fumarate to L-malate in the TCA cycle, while the cytosolic form catalyses
241 dehydration of L-malate to fumarate[29,30]. Two isoforms exist in *C. reinhardtii*, FUM1
242 encoded in locus Cre06.g254400 and FUM2. Based on the predicted subcellular localisation
243 (PredAlgo; http://lobosphaera.ibpc.fr/cgi-bin/predalgodb2.perl?page=main), FUM1 localizes
244 to the mitochondria, while FUM2 is assigned to the "other" compartment and is likely to be a
245 cytosolic protein. Pathway (KEGG) diagrams for the TCA cycle and pyruvate metabolism
246 can be found in Supplementary Fig. 6, showing integration of metabolite, RNA-seq and qRT-
247 PCR data. Comparison of the transcriptomes of *gunSOS1* and *sigRep* also indicated increased
248 expression of the *FUMARYLACETOACETASE* gene (locus *Cre17.g732802*, EC 3.7.1.2)
249 involved in tyrosine catabolism. FUMARYLACETOACETASE catalyses hydrolysis of 4-
250 fumarylacetoacetate to acetoacetate and fumarate (Supplementary Fig. 7). Increased
251 expression of genes encoding FUM2 and FUMARYLACETOACETASE could explain
252 accumulation of fumarate in *gunSOS1* compared to *sigRep*.
253 Aconitate deficiency in *gunSOS1* compared to *sigRep* can be explained by
254 transcriptional downregulation of *ACONITATE HYDRATASE* (*ACH1*, Cre01.g042750,
255 EC 4.2.1.3). ACH1 interconverts citrate and isocitrate, via cis-aconitate, in the TCA cycle
256 (Supplementary Fig. 8) and is also involved in glyoxylate and dicarboxylate metabolism. At
257 equilibrium, the reactants of the ACH1 reaction are present in the following ratio: 91%
258 citrate, 6% isocitrate and 3% aconitate. With the smallest pool of the three tricarboxylic
259 acids, fluctuations in the level of aconitate are expected to be more pronounced compared to
260 the other metabolites involved, especially citrate, whose content was similar in *gunSOS1* and
261 *sigRep* in the light (Supplementary Fig. 5). Taken together, our data indicate that altered
262 fumarate and aconitate content in *gunSOS1* compared to *sigRep* can be explained by altered
263 expression of genes encoding enzymes involved in key metabolic processes affecting those
264 metabolites.
265
266 **Impaired $^1O_2$-signalling in *gunSOS1* correlates with decreased expression of *PSBP2*,**
267 ***MBS*, and *SAK1***
268 The PSBP2[14], MBS[16], and SAK1[15] proteins are required for $^1O_2$-induced chloroplast
269 retrograde signalling in *C. reinhardtii*. Therefore, we determined the transcript levels of
270 *PSBP2*, *MBS*, and *SAK1*, which were 8-, 9-, and nearly 41-fold lower, respectively, in
271 *gunSOS1* compared to *sigRep* (Fig. 7a). Decreased expression of *SAK1* in *gunSOS1* prompted
272 us to compare transcript levels of selected $^1O_2$-responsive genes between *gunSOS1* and *sak1*,

273 which lacks acclimation response to $^1O_2$[15]. SAK1 is a key regulator of the gene expression
274 response and its involvement in $^1O_2$-signalling was determined following treatment with rose
275 bengal[15], which produces $^1O_2$ in the light. Nevertheless, based on our qRT-PCR analysis, all
276 tested genes had the same reduced inducibility in *gunSOS1* compared to *sigRep* (Fig. 7b), as
277 it was observed in *sak1* compared to WT following $^1O_2$-exposure[15]. Among the genes that
278 were down-regulated in both *gunSOS1* (Fig. 7b) and *sak1*[15] were two *CYCLOPROPANE*
279 *FATTY ACID SYNTHASES*, *CFA1* and *CFA2* (*CPLD27*), involved in lipid and sterol
280 metabolism, as well as the gene encoding SOUL1 heme-binding protein (Fig. 7b). It is
281 noteworthy that attenuated expression of both *CFA1* and *CFA2*, as well as *SOUL1*, was also
282 observed in studies on a *gpx5* mutant[31]. Furthermore, in agreement with the *sak1* phenotype
283 presented in Wakao, et al. [15], *gunSOS1* also showed decreases in transcript content of
284 *PEPTIDE METHIONINE SULFOXIDE REDUCTASE* (*MSRA3*), *ALCOHOL*
285 *DEHYDROGENASE* (*ADH7*), *RETINALDEHYDE BINDING PROTEIN-RELATED*
286 (*RABPR2*), and Cre01.g007300 encoding N-
287 ACETYLPHOSPHATIDYLETHANOLAMINE-HYDROLYZING PHOSPHOLIPASE D
288 (Fig. 7b). Thus, there is an overlap between the phenotypes of *gunSOS1* and *sak1*[15] with
289 respect to their attenuated expression of genes induced during elevated $^1O_2$ (Fig. 7b).
290

291 **Altered metabolite content affects $^1O_2$-signalling**

292 We hypothesized that at least some of the metabolites showing increased or decreased
293 content in *gunSOS1* compared to *sigRep*, attenuate or propagate $^1O_2$-signalling, respectively.
294 We selected fumarate and aconitate as representatives of either group. To test our hypothesis,
295 metabolites were added separately to the liquid cultures at empirically determined sublethal
296 concentrations, followed by incubation in the light to induce $^1O_2$ generation by Proto.
297 Subsequently, the $GPX5_{cyt}$ and $GPX5_{cp}$ transcript levels were used as readouts for the $^1O_2$
298 signalling efficiency in *gunSOS1* and *sigRep*.

299 Exogenous application of fumarate significantly ($P < 0.001$, a detailed report from
300 two-way ANOVA analyses is presented in Supplementary Tables 4 and 5) attenuated
301 expression of both $GPX5_{cyt}$ and $GPX5_{cp}$ in a concentration-dependent manner in *sigRep* (Fig.
302 8a). As expected, fumarate did not affect *GPX5* expression in *gunSOS1*. Application of 20
303 µM aconitate significantly ($P < 0.0001$) increased expression of *GPX5* in *gunSOS1* and even
304 further in *sigRep* compared to untreated cells ($P < 0.0001$), but 100 µM had a quenching
305 effect on the *GPX5* expression in *sigRep* (Fig. 8b, Supplementary Tables 6 and 7). This
306 indicates that aconitate up to a certain threshold concentration promotes $^1O_2$ signalling.

307 Subsequently, we determined the expression of *SAK1* upon feeding *gunSOS1* and
308 *sigRep* with aconitate. Exogenous application of aconitate at 20 µM increased *SAK1*
309 transcript abundance in *gunSOS1* more than 120 times compared to the untreated *gunSOS1*
310 control, and exceeded values observed in *sigRep* subjected to the same treatment by a factor
311 of 5 (Fig. 8c). Due to the increased *SAK1* expression in *gunSOS1* upon feeding with
312 aconitate, we also determined the expression of *PSBP2* and *MBS* in the same conditions. The
313 *PSBP2* response to aconitate was similar to *SAK1* in terms of the increased expression (Fig.
314 8c), but with less pronounced dependence on the metabolite concentration compared to
315 *SAK1*. Although 20 µM aconitate increased *PSBP2* expression in *gunSOS1* by a factor of 48
316 compared to the untreated control, it was still 2.7 times lower compared to *sigRep* subjected
317 to the same treatment (Fig. 8c). Similarly to *SAK1* and *PSBP2*, 20 µM aconitate also
318 increased expression of *MBS* in *gunSOS1*, although values did not exceed those observed in
319 *sigRep* subjected to the same treatment (Fig. 8c). Statistical analyses indicated that the effect
320 of 20 µM aconitate on *SAK1*, *PSBP2* and *MBS* expression in *sigRep* and *gunSOS1*,
321 interaction between mutants and aconitate, as well as the mutant-dependent expression of
322 these genes were always significant ($P < 0.001$, Supplementary Tables 8-10).
323
324 **Specificity of the $^1O_2$-signalling pathway(s) attenuated in *gunSOS1***
325 The profound effect of accumulating Tre6P on the transcriptome (Fig. 6a-c) and consequently
326 the metabolism of *gunSOS1* (Fig. 3 and Fig. 4) may have been indicative of a general
327 photooxidative stress response being impaired in *gunSOS1*. To determine the specificity of
328 this response, we compared *gunSOS1* and *sigRep* in terms of the expression of selected genes
329 that are known to be induced by various reactive species or conditions causing
330 photooxidative stress other than $^1O_2$.
331 Upon H_2O_2 or organic *tert*-butyl hydroperoxide (*t*-BOOH) treatment, Blaby, et al. [32]
332 observed an increase in the expression of the *MSD3* gene, encoding plastid-localised Mn
333 SUPEROXIDE DISMUTASE 3. In our studies, we did not observe an increase in *MSD3*
334 transcript in *sigRep* compared to WT (Fig. 9a), which shows that *MSD3* expression is not
335 inducible by $^1O_2$ produced by Proto. However, based on qRT-PCR analysis, a 9-fold increase
336 was observed in *gunSOS1* compared to *sigRep* (Fig. 9a, see also RNA-seq in Supplementary
337 Data Set 2). Upon H_2O_2 or *t*-BOOH treatment, Urzica, et al. [33] also observed induced
338 expression of genes involved in the glutathione-ascorbate system, *GDP-L-GALACTOSE*
339 *PHOSPHORYLASE* (*VTC2*) and *DEHYDROSASCORBATE REDUCTASE* (*DHAR1*). Based
340 on our qRT-PCR results, *VTC2* transcript content was not changed in *sigRep* compared to

341 WT, but an increase was observed in *gunSOS1* (Fig. 9b; Supplementary Data Set 2). *DHAR1*
342 expression was also stimulated in *gunSOS1* compared to *sigRep* (Fig. 9c; Supplementary
343 Data Set 2).

344 Similarly to *sak1* following treatment with rose bengal[15], we observed increased
345 expression of *GLUTATHIONE S-TRANSFERASE* (*GSTS1*) in *gunSOS1* compared to *sigRep*
346 (Fig. 9d, Supplementary Data Set 2). However, in another study increased expression of
347 *GSTS1* was shown after treatment with acrolein, which suggests its transcriptional induction
348 by reactive electrophile species (RES)[34]. Acrolein was also shown to induce *FSD1* encoding
349 Fe SUPEROXIDE DISMUTASE (FeSOD[34], which was expressed both in *sigRep* and
350 *gunSOS1* (Supplementary Data Set 1), and no significant difference could be observed in
351 DEG analysis (Supplementary Data Set 2) or qRT-PCR (Fig. 9e). It can be concluded that,
352 despite impaired $^1O_2$-signalling, *gunSOS1* retained the ability to respond to photooxidative
353 stress caused by other ROS such as H_2O_2, organic peroxides, or RES.

354

355 **Discussion**

356 ROS are formed as a by-product of biological redox reactions[35] mostly in the mitochondria or
357 chloroplasts[36,37]. Although excess ROS production can cause oxidative damage to cell
358 components, ROS or the oxidation products play an important role in the signal transduction
359 processes.

360 Different retrograde signalling pathways have been proposed to involve also TBS-
361 intermediates in plants and green algae (reviewed in[38,39]). While involvement of Mg-
362 porphyrins in chloroplast retrograde signalling is now excluded[40,41], in the present study we
363 have demonstrated that $^1O_2$ produced by the photosensitizing activity of Proto in the light, but
364 not Proto itself, triggers signalling cascades that alter nuclear gene expression. Using strains
365 that endogenously accumulate Proto, we identified several mutants that are impaired in $^1O_2$-
366 signalling. Endogenous accumulation of Proto in mutants is advantageous for studying $^1O_2$-
367 signalling, because it eliminates the need for exogenous application of TBS or carotenoid
368 biosynthesis inhibitors, as well as photosensitizers, such as rose bengal or neutral red (Fischer
369 et al., 2004) to induce $^1O_2$ generation. The lack of chlorophyll provides another advantage,
370 because such mutants do not have functional photosynthetic electron transport, so that $^1O_2$
371 production in photosynthesis is avoided. The accumulating Proto is thus the dominant source
372 of generated $^1O_2$.

373 The $^1O_2$-induced signalling phenotype in the *gunSOS1* mutant was due to a lesion in
374 the *T6PP1* gene. We demonstrated that T6PP1 is a functional phosphatase capable of

375 dephosphorylating Tre6P. *T6PP1* is the only representative of the classical plant *TPP* gene
376 family in *C. reinhardtii*, contrasting with the large *TPP* gene families in angiosperms[42]. In
377 addition, *C. reinhardtii* has one representative of the class I *TREHALOSE-6-PHOSPHATE*
378 *SYNTHASE* (*TPS*) family (Cre16.g662350, hereafter *T6PS1*), and two members of the class II
379 *TPS* family (Cre06.g278221, here *T6PSP1* and Cre16.g686200, here *T6PSP2*). Both class I
380 and class II TPS proteins have glucosyltransferase and TPP-like domains, but only the class I
381 TPS proteins have demonstrated TPS activity[43-45]. T6PP1 belongs to the haloacid
382 dehalogenase superfamily of proteins and contains the characteristic DXDX(T/V) active site
383 motif – $_{107}$DYDGT$_{112}$ – in which the initial Asp residue forms a phospho-acyl intermediate
384 during catalysis[46]. T6PSP1 also contains the complete active site motif ($_{592}$DYDGT$_{597}$), so we
385 cannot exclude the possibility that the T6PSP1 protein in *C. reinhardtii* has TPP activity,
386 which could explain the increased content of trehalose in *gunSOS1* compared to *sigRep*.
387 Although the intracellular localizations of these proteins have not been determined
388 experimentally in *C. reinhardtii*, PredAlgo analysis indicated possible localization of T6PP1
389 and T6PSP1 in mitochondria, while T6PS1 and T6PSP2 are likely to be cytosolic proteins,
390 because they were not assigned to any specific organelle.

391 Correlation between *T6PP1* (Fig. 2b) and *GPX5* (Fig. 1b, c) expression indicates that
392 low Tre6P content is required for efficient $^1O_2$-signalling. However, the apparent negative
393 effect of Tre6P on $^1O_2$-signalling is not direct and involves a complex metabolic
394 reprogramming (Fig. 10). Study on the contrasting phenotypes between *A. thaliana*
395 overexpressing bacterial TPS, TPP, or TREHALOSE PHOSPHATE HYDROLASE (TPH)
396 pointed to Tre6P, rather than trehalose, playing a signalling function[25]. Tre6P was shown to
397 be highly correlated with sucrose, leading to the proposal that it functions as a signal of
398 sucrose status[23]. Tre6P was also shown to inhibit starch degradation in *A. thaliana*[47,48], which
399 is also true in Tre6P-acumulating *gunSOS1* mutant of *C. reinhardtii*.

400 It was demonstrated that Tre6P acts as an inhibitor of SUCROSE-NON-
401 FERMENTING (SNF)-RELATED PROTEIN KINASE1 (SnRK1) in developing tissues and
402 that this is dependent on a so-far unidentified protein factor[49-51]. Tre6P also inhibits the
403 activation of SnRK1 by SnRK1-activating kinases/geminivirus Rep interacting kinases[52].
404 SnRK1 belongs to the AMPK-SNF1-SnRK family of protein kinases, which is represented in
405 all eukaryotes[53]. In plants, SnRK1 plays a central role in energy and metabolic homeostasis,
406 and is activated during energy deficient conditions caused by stresses like nutrient starvation,
407 pathogen attack, or ROS[54]. Baena-González, et al. [55] established approximately 1000 genes as
408 markers of SnRK1 in *A. thaliana*, which indicates an extensive SnRK1-dependent

409 transcriptional reprogramming. In *C. reinhardtii*, involvement of various SnRKs in responses
410 to stress was observed during sulphur[56,57] and nitrogen deprivation[58], or cold stress[59].
411 Genome-wide analysis revealed the existence of 21 genes as potential orthologues of the
412 plant SnRK α, β and γ/βγ subunits in *C. reinhardtii*. It was suggested that the proteins
413 encoded by these genes play the same role in cell survival and stress response in *C.*
414 *reinhardtii* as SnRKs in land plants[58].

415 In analogy to *A. thaliana*, altered SnRKs activity was shown to cause metabolic
416 remodelling also in algae[59]. In our study, the majority of changes to gene expression observed
417 in *gunSOS1*, relative to *sigRep*, originates from accumulation of Tre6P and, based on
418 previous studies, this leads to inhibition of one or more SnRKs (Fig. 10). Our analysis
419 showed that altered gene expression in *gunSOS1* relative to *sigRep* (Supplementary Fig. 6-8)
420 is directly responsible for altered fumarate and aconitate content in *gunSOS1* compared to
421 *sigRep*. Thus, Tre6P accumulating in *gunSOS1* is not directly involved in $^1O_2$-signalling but
422 controls other processes in the cell which affect $^1O_2$-signalling more directly (Fig. 10).

423 We demonstrated that accumulation of fumarate is responsible for attenuating $^1O_2$-
424 signalling (Fig. 8a, Fig. 10). Fumarate is a well-recognized oncometabolite in mammalian
425 cells[60], associated with development of tumours by competitive inhibition of 2-oxoglutarate-
426 dependent oxygenases, including HYPOXIA INDUCIBLE FACTOR (HIF) hydroxylases,
427 leading to stabilisation of HIF and activation of oncogenic HIF-dependent pathways[61]. In
428 fact, accumulation of fumarate in human cells was linked to an aggressive variant of
429 hereditary kidney cancer[62]. In mice, fumarate was also shown to directly modify some
430 proteins by succination of cysteine residues to form 2-succinocysteine derivatives[63].
431 Succination of three cysteines crucial for iron-sulphur cluster binding was identified in
432 mitochondrial ACONITASE2 (ACO2) in a *fumarate hydratase 1* knockout (Fh1KO) mouse
433 embryonic fibroblast (MEF) cell line[63]. Analysis of tryptic peptides derived from ACO2 in
434 Fh1KO MEFs, indicated succination of Cys385. Another tryptic peptide of ACO2 was
435 identified as a mixture of two isomers in Fh1KO MEFs, which showed succination at Cys451
436 or Cys448[63]. Succination of these cysteine residues in ACO2 leads to its inhibition[63].
437 Equivalent cysteine residues are conserved in *C. reinhardtii* ACH1, which explains the
438 aconitate deficiency in *gunSOS1* (Fig. 4a).

439 The *gunSOS1* mutant showed decreased levels of aconitate compared to *sigRep*, while
440 exogenous application of this metabolite to *gunSOS1* restored $^1O_2$-signalling. Mammalian
441 ACO2 is thought to be a mitochondrial oxidative stress sensor, which requires an active
442 $[Fe_4S_4]^{2+}$ cluster[64]. It is, therefore, proposed that accumulation of fumarate deactivates ACH1

443 and reduces the aconitate content in *gunSOS1*, thereby impairing oxidative stress sensing and
444 $^1O_2$-signalling. Diminished expression of *ACH1* in *gunSOS1* relative to *sigRep*
445 (Supplementary Fig. 8a, b) may be an additional factor adding to the aconitate depletion in
446 *gunSOS1*.

447 Results obtained in our study indicate that there is a metabolic signature conditioning
448 $^1O_2$-signalling. A mechanism in which the chloroplast controls nuclear gene expression via
449 metabolite levels was postulated before[12,65]. It was shown that altered chloroplast redox
450 conditions result in changes in the metabolome in *A. thaliana*, reflected also by the
451 reallocation of energy resources[66]. Importantly, although our study shows that the metabolic
452 configuration of the cell is essential for $^1O_2$-signalling, this does not exclude the involvement
453 of protein components in this signalling network (Fig. 10). On the contrary, our findings
454 support the direct involvement of proteins in $^1O_2$-signalling, but we demonstrated that
455 expression of *PSBP2*[14], *MBS*[16], and *SAK1*[15] depends on the metabolic status (Fig. 7a and Fig.
456 8a, b). The overlap between the *gunSOS1* and the SAK1-dependent transcriptomes (Fig. 7b)
457 as well as other defined ROS or RES-dependent signalling pathways being functional (Fig.
458 9a-e) indicate specificity of the impaired $^1O_2$-signalling in *gunSOS1*. Our results indicate that
459 fumarate and aconitate affect the expression of *PSBP*, *MBS*, or *SAK1*, which subsequently
460 convey information about the metabolic status of the cell to the nucleus and trigger specific
461 responses (Fig. 10). It is not clear yet how the specificity of the signalling is achieved,
462 because the mechanisms by which metabolites affect the expression of these proteins, as well
463 as downstream components of these signalling pathways, remain unknown. Additionally, the
464 protein components involved in $^1O_2$-signalling may be subject to additional regulatory
465 mechanisms, such as phosphorylation, as proposed for SAK1 by Wakao, et al. [15].

466 We have shown that retrograde signalling triggered by $^1O_2$, which is mostly generated
467 in the chloroplast, strictly depends on the mitochondrial metabolic status. PROLYL-tRNA
468 SYNTHETASE (PRORS1) in *A. thaliana*, a component of the organellar gene expression
469 machinery indicated that mitochondria may contribute to chloroplast retrograde signalling[67].
470 PRORS1 is targeted both to the plastid and to mitochondria, but downregulation of specific
471 photosynthesis-associated nuclear genes was observed only in a plastidial *prpl11* and
472 mitochondrial *mrpl11* double mutant, but not in *prpl11* or *mrpl11* single mutants[67]. Another
473 study showed that the ROS-dependent signals from chloroplast and mitochondria are
474 integrated at the RADICAL-INDUCED CELL DEATH 1 (RCD1) protein located in the
475 nucleus[68]. RCD1 suppresses transcription factors ANAC013 and ANAC017, which mediate
476 the ROS-signal from mitochondria, while chloroplast regulation of RCD1 takes place through

477 3'-phosphoadenosine 5'-phosphate. It was proposed that RCD1 may function at the
478 intersection of mitochondrial and chloroplastic retrograde signalling pathways[68] .
479 The retrograde signalling pathways identified so far assume the existence of separate
480 signalling routes. However, chloroplast retrograde signalling involves a network of different
481 but inter-connected mechanisms, and observation of specific signalling pathways within the
482 network depends on the experimental conditions. Pharmacological or genetic interventions
483 that disrupt specific pathways can be used to characterize alternative pathways. In the
484 manuscript presented here, we report that the metabolic status of the cell, reflecting levels of
485 Tre6P, and components of the mitochondrial TCA cycle are integral factors in the $^1O_2$-
486 dependent retrograde signalling network in *C. reinhardtii*.
487
488 **Methods**
489 ***Chlamydomonas reinhardtii* cultures and genetic manipulations**
490 All strains were cultivated heterotrophically in Tris-acetate-phosphate (TAP) medium in the
491 dark. Additionally, starch measurements were performed in TAP, Tris-phosphate (TP)
492 medium without acetate, or nitrogen-depleted (TAP-N) medium. Experiments were
493 performed in TAP medium in the dark or upon a shift to 20 µmol photons m^{-2} s^{-1} light. Three
494 strains used in this study were described elsewhere, *chlD-1* in von Gromoff, et al. [17], *chlD-*
495 *1/GUN4* in Brzezowski, et al. [18], and wild type (4A+) in Dent, et al. [69].
496 To generate the *GPX5-ARS2* construct (Supplementary Fig. 2), the *GPX5* regulatory
497 region (*GPX5* 5' RR) was amplified by PCR using forward and reverse primers carrying
498 XhoI and EcoRV restrictions sites, respectively (Supplementary Table 11**)**. The obtained
499 fragment was subcloned and ligated between the XhoI/EcoRV sites of the pSL18 vector[70],
500 replacing the existing promoter region of the gene encoding the PSAD and positioning *GPX5*
501 5'RR in reverse orientation with respect to the paromomycin resistance cassette (paro[R,71]. The
502 DNA fragment carrying paro[R] and *GPX5* 5' RR was excised by restriction digestion with
503 KpnI and EcoRV and ligated into the corresponding restriction sites of pJD54[72], which
504 carries a copy of the promoterless version of the gene encoding ARYLSULFATASE 2
505 (ARS2), which allowed *ARS2* expression to be controlled by the *GPX5* 5'RR (Supplementary
506 Fig. 2). The *GPX5-ARS2* construct was verified by sequencing.
507 The *sigRep* strain was produced in the *chlD-1/GUN4* background by transformation
508 with a *GPX5-ARS2* construct. Transformant selection was performed on TAP agar plates with
509 10 µg mL^{-1} paromomycin in dark, followed by a screen for *GPX5-ARS2* inducibility by $^1O_2$.
510 The *sigRep* strain showed low ARS2 activity in the dark and high activity in the light (Fig.

511 1a) and was selected for further applications. The *gunSOS1* mutant was generated by random
512 insertional mutagenesis performed on *sigRep* using a bleomycin resistance cassette (ble^R)
513 isolated from the pMS188 vector[73] using NotI and KpnI. Following mutagenesis, selection
514 was performed on TAP agar plates containing 15 µg mL^{-1} zeocin in the dark. More than 800
515 obtained colonies were screened for decreased or not detectable ARS2 activity in the light
516 and nine mutants that showed impaired inducibility of *GPX5-ARS* expression in light were
517 selected for further analysis. Restriction enzyme site-directed amplification PCR[74] allowed
518 us to identify the genomic DNA flanking the ble^R insertion sites in five out of the nine
519 mutants. Only analysis of the *gunSOS1* mutant is presented here. Rescue of *gunSOS1* (*t6pp1*)
520 was conducted with 5242 bp fragment of genomic DNA carrying 3241 bp *T6PP1* amplified
521 by PCR (see Supplementary Table 11 for primers) using bacterial artificial chromosome
522 PTQ5987 (Clemson University Genomics Institute, Clemson, SC, USA) as a template. The
523 amplified DNA fragment included 1500 bp upstream and 501 bp downstream of the
524 annotated *T6PP1*. Wild-type *T6PP1* was introduced into *gunSOS1* by co-transformation with
525 a spectinomycin resistance cassette isolated from the pALM32 vector[75] with AleI and KpnI
526 endonucleases. Transformant selection was performed on TAP agar plates supplemented with
527 100 µg mL^{-1} spectinomycin in the dark. All genetic transformations were performed by
528 electroporation.
529
530 **Arylsulfatase activity assay**
531 To assess the level of *GPX5-ARS2* expression in transformed cells, enzymatic assays
532 for arylsulfatase activity[76] were performed essentially as described before[14]. Cells were
533 spotted onto agar-solidified TAP medium plates and cultured in either light or dark
534 conditions. Arylsulfatase is expected to be secreted into the medium if *GPX5-ARS2* is
535 expressed. After removal of the cells, plates were flooded with detection solution containing
536 0.1 mg mL^{-1} 2-naphthyl sulfate (potassium salt; Santa Cruz Biotechnology, Inc., Dallas, TX,
537 USA) as a chromogenic substrate coupled with 1 mg mL^{-1} tetrazotized-o-dianisidine chloride
538 (Fast Blue B salt, Santa Cruz Biotechnology, Inc., Dallas, TX, USA). Following 1 h
539 incubation, purple spots appearing on the agar plates identified expressed ARS2.
540
541 **Analysis of protoporphyrin IX content**
542 The Proto content was analysed by High Pressure Liquid Chromatography (HPLC)
543 essentially as described in Czarnecki, et al. [77], with modified sample preparation for *C.*
544 *reinhardtii*[18]. In short, cultures were grown in the dark and transferred to 20 µmol photons m^-

545 ^{2} s^{-1} light for 2 h. Samples containing 1.2×10^8 cells were centrifuged at 3000 x *g* for 5 min at
546 4°C and the pellets were snap-frozen in liquid N_2. Proto was extracted in cold (-20°C)
547 acetone/0.1 M NH_4OH (9/1, v/v) in a three-step cycle of resuspension and centrifugation.
548 Proto analysis was performed using a Nova-Pak C18 column (Waters, 3.9 × 150 mm, 4 µm,
549 at 20 °C). The results were normalized to pmol/10^6 cells.
550
551 **RNA isolation, qRT-PCR, and RNA-seq**
552 The total RNA was isolated, after a shift from dark to 20 µmol photons m^{-2} s^{-1} light for 2 h,
553 using TRIzol Reagent (Thermo Fisher Scientific, Waltham, MA, USA), according to the
554 manufacturer's protocol. RNA quality was assessed by electrophoresis on a 1% (w/v) agarose
555 gel, while quantity was determined using a Nanodrop 2000 (Thermo Fischer Scientific,
556 Waltham, MA). Aliquots of 2 µg RNA were treated with DNase and RiboLock RNase
557 inhibitor (Thermo Fisher Scientific, Waltham, MA, USA) and used to synthesize cDNA with
558 RevertAid Reverse Transcriptase (Thermo Fisher Scientific, Waltham, MA, USA) and
559 oligo$(dT)_{18}$ primer. Transcript analysis by qRT-PCR were performed using 2× ChamQ
560 Universal SYBR qPCR Master Mix (Viazyme Biotech Co., Ltd., Nanjing, China) and a
561 CFX96-C1000 96-well plate thermocycler (Bio-Rad, Hercules, CA, USA), the 18S rRNA
562 was used as a reference gene[22]. All primers were designed using Primer3Plus
563 (http://primer3plus.com), and are listed in Supplementary Table 11.
564 RNA-sequencing was performed on total RNA samples isolated from biological
565 triplicates of *sigRep* and *gunSOS1* after the shift from dark to 20 µmol photons m^{-2} s^{-1} light
566 for 2 h. Library preparation, sequencing, and analysis services were commercially provided
567 by Novogene Europe (Novogene (UK) Company Ltd., Cambridge, UK) and performed using
568 an Illumina NovaSeq 6000 platform operated in 150 bp pair end sequencing mode, with a
569 sequencing depth of 20 million reads per sample. Six gigabases of sequencing data per library
570 was filtered for high-quality reads, which were mapped to the *C. reinhardtii* v5.5
571 (Department of Energy JGI). Estimated expression was obtained in fragments per kilobase of
572 transcript sequence per millions base pairs sequenced (FPKM). Biological replicates were
573 averaged to obtain sample expression estimate. Differential expression analysis between two
574 mutants (three biological replicates per mutant) was performed using DESeq2.v1.20.0, which
575 provides statistical routines for determining differential expression using a model based on
576 the negative binomial distribution. The resulting *p* values were adjusted using the Benjamini
577 and Hochberg's approach for controlling the False Discovery Rate (FDR). Genes with a
578 $\log_2$FoldChange ≥ 2 and adjusted *p* value (padj) < 0.05 found by DESeq2.v1.20.0 were

579 defined as differentially expressed (DEGs). Gene Ontology (GO) analysis and Kyoto
580 Encyclopedia of Genes and Genomes (KEGG; www.genome.jp/kegg/pathway.html) pathway
581 analysis were conducted to identify DEGs at the biologically functional level using
582 clusterProfiler R package. GO terms and KEGG pathways with a padj < 0.05 were
583 considered to be significantly enriched.
584
585 **Metabolite analysis**
586 Cultures were grown in TAP in the dark until they reached mid-log phase of 3 x 10^6 cells mL^{-}
587 ^{1}. Samples were always normalized to contain 6 x 10^7 cells, all centrifugation steps were
588 carried at 3000 x *g* at 4°C for 5 min, followed by snap-freezing in liquid N_2. Samples from
589 dark conditions were collected immediately, while the remainder of each culture was
590 transferred to 20 µmol photons m^{-2} s^{-1} light. Subsequent sampling took place at 15-min
591 intervals, up to 1 h. Metabolites were extracted using chloroform-methanol as described by
592 Lunn et al. (2006). Tre6P, other phosphorylated intermediates and organic acids were
593 measured by anion-exchange HPLC coupled to tandem mass spectrometry (LC-MS/MS) as
594 described in Lunn et al. (2006) with modifications as described in[78]. Sugars and sugar
595 alcohols were measured by LC-MS/MS as described in[79]. Obtained results were normalized
596 to pmol/10^6 cells.
597 For starch analysis, cultures were grown in TAP in the dark until they reached mid-
598 log phase of 3 x 10^6 cells mL^{-1}. For starch determination cultures were either transferred in
599 TAP to the light (20 µmol photons m^{-2} s^{-1}) for 2 h before harvesting, or centrifuged cells were
600 resuspended in Tris-phosphate (TP) medium (without acetate), keeping the same cell
601 concentration, and transferred back to the dark for 24 h. Subsequently, cultures were
602 transferred to 20 µmol photons m^{-2} s^{-1} for 2 h before harvesting. A similar protocol was
603 applied for starch analysis in TAP devoid of N (TAP-N), except that cells were cultivated in
604 TAP-N for 3 days in the dark, followed by exposure to 20 µmol photons m^{-2} s^{-1} for 2 h. For
605 each sampling, 5 x 10^6 cells were centrifuged and lyophilized. Starch content was determined
606 by enzymatic degradation and glucose quantification following the protocol of DuBois, et al.
607 [80].
608
609 **Protein extraction and immunoblot analysis**
610 Cultures were grown in the dark, followed by a transfer to 20 µmol photons m^{-2} s^{-1} for 3 h.
611 Cells were pelleted by centrifugation and total proteins were extracted in 400 µL buffer
612 containing: 56 mM Na_2CO_3, 56 mM DTT, 2% (w/v) SDS, 12% (w/v) sucrose and 2 mM

613 EDTA, pH 8.0. Proteins were quantified using Pierce™ BCA Protein Assay Kit (Thermo
614 Fisher Scientific, Waltham, MA, USA) and separated by SDS-PAGE on a 12%
615 polyacrylamide gel, followed by transfer by electroblotting to nitrocellulose membrane (GE
616 Healthcare, Chicago, IL, USA). T6PP1 was detected using a rabbit crude antiserum (dilution
617 1:500) raised by inoculation with a T6PP1-specific peptide (VEWSKSDSNGWRAKPC)
618 against *C. reinhardtii* T6PP1 (calculated MW 42 kDa). GPX5 was detected with a
619 commercially available antibody (AS15 2882, dilution 1:1000) obtained from Agrisera
620 (Vännäs, Sweden). CHLI1 antibody (PHY5510S, dilution 1:1000) was purchased from
621 PhytoAB (San Jose, CA, USA). For application, all antibodies were diluted in CrossDown
622 buffer (AppliChem, AppliChem GmbH, Darmstadt, Germany). The secondary antibody
623 (AS09 602, goat anti-rabbit IgG, dilution 1:10,000) conjugated to horseradish peroxidase was
624 obtained from Agrisera. The immunoblotting signals were detected using a CCD camera
625 (Intas Biopharmaceuticals, Ahmedabad, India) after application of enhanced
626 chemiluminescence detection kit (Clarity™ Western ECL Substrate; Bio-Rad, Hercules, CA,
627 USA.
628
629 **Chemical treatments of *C. reinhardtii* cells**
630 Fumarate (sodium fumarate dibasic) and aconitate (*cis*-aconitic acid) were obtained from
631 Sigma-Aldrich (Sigma-Aldrich Chemie GmbH, Taufkirchen, Germany), dissolved in H_2O to
632 a stock solution of 100 mM and added individually to the mid-log phase (3 x 10^6 cells mL^{-1})
633 cultures to final concentrations of 20, 50, and 100 μM, followed by exposure to light for 2 h.
634
635 **Data availability statement**
636 The data that support the findings of this study are available from the corresponding author
637 upon reasonable request.
638
639 **References**
640 1 Johanningmeier, U. & Howell, S. H. Regulation of light-harvesting chlorophyll-binding
641 protein mRNA accumulation in *Chlamydomonas reinhardii*. Possible involvement of
642 chlorophyll synthesis precursors. *J. Biol. Chem.* **259**, 3541-3549 (1984).
643 2 Oelmüller, R. Photooxidative destruction of chloroplasts and its effect on nuclear gene
644 expression and extraplastidic enzyme levels. *Photochem. Photobiol.* **49**, 229-239,
645 doi:10.1111/j.1751-1097.1989.tb04101.x (1989).
646 3 Susek, R. E., Ausubel, F. M. & Chory, J. Signal transduction mutants of Arabidopsis
647 uncouple nuclear CAB and RBCS gene expression from chloroplast development. *Cell* **74**,
648 787-799 (1993).

649 4 Oster, U., Brunner, H. & Rudiger, W. The greening process in cress seedlings .5. Possible
650 interference of chlorophyll precursors, accumulated after thujaplicin treatment, with light-
651 regulated expression of Lhc genes. *J. Photoch. Photobio. B* **36**, 255-261, doi:10.1016/s1011-
652 1344(96)07388-5 (1996).
653 5 Lydon, J. & Duke, S. O. Porphyrin synthesis is required for photobleaching activity of the
654 para-nitrosubstituted diphenyl ether herbicides. *Pestic. Biochem. Physiol.* **31**, 74-83,
655 doi:10.1016/0048-3575(88)90031-4 (1988).
656 6 Triantaphylides, C. *et al.* Singlet oxygen is the major reactive oxygen species involved in
657 photooxidative damage to plants. *Plant Physiol.* **148**, 960-968, doi:10.1104/pp.108.125690
658 (2008).
659 7 op den Camp, R. G. L. *et al.* Rapid induction of distinct stress responses after the release of
660 singlet oxygen in Arabidopsis. *Plant Cell* **15**, 2320-2332, doi:10.1105/tpc.014662 (2003).
661 8 Baruah, A., Simkova, K., Apel, K. & Laloi, C. Arabidopsis mutants reveal multiple singlet
662 oxygen signaling pathways involved in stress response and development. *Plant Mol. Biol.* **70**,
663 547-563, doi:10.1007/s11103-009-9491-0 (2009).
664 9 Gorman, A. A. & Rodgers, M. A. J. Current perspectives of singlet oxygen detection in
665 biological environments. *J. Photoch. Photobio. B* **14**, 159-176 (1992).
666 10 Beck, C. F. Signaling pathways from the chloroplast to the nucleus. *Planta* **222**, 743-756,
667 doi:10.1007/s00425-005-0021-2 (2005).
668 11 Sies, H. & Menck, C. F. M. Singlet oxygen induced DNA damage. *Mutat. Res.* **275**, 367-375
669 (1992).
670 12 Pfannschmidt, T. Plastidial retrograde signalling - a true "plastid factor" or just metabolite
671 signatures? *Trends Plant Sci.* **15**, 427-435, doi:10.1016/j.tplants.2010.05.009 (2010).
672 13 Kim, C. *et al.* Chloroplasts of Arabidopsis are the source and a primary target of a plant-
673 specific programmed cell death signaling pathway. *Plant Cell* **24**, 3026-3039,
674 doi:10.1105/tpc.112.100479 (2012).
675 14 Brzezowski, P., Wilson, K. E. & Gray, G. R. The PSBP2 protein of Chlamydomonas
676 reinhardtii is required for singlet oxygen-dependent signaling. *Planta* **236**, 1289-1303,
677 doi:10.1007/s00425-012-1683-1 (2012).
678 15 Wakao, S. *et al.* Phosphoprotein SAK1 is a regulator of acclimation to singlet oxygen in
679 Chlamydomonas reinhardtii. *eLife* **3**, e02286, doi:10.7554/eLife.02286 (2014).
680 16 Shao, N., Duan, G. Y. & Bock, R. A mediator of singlet oxygen responses in
681 Chlamydomonas reinhardtii and Arabidopsis identified by a luciferase-based genetic screen in
682 algal cells. *Plant Cell* **25**, 4209-4226, doi:10.1105/tpc.113.117390 (2013).
683 17 von Gromoff, E. D., Alawady, A., Meinecke, L., Grimm, B. & Beck, C. F. Heme, a plastid-
684 derived regulator of nuclear gene expression in *Chlamydomonas*. *Plant Cell* **20**, 552-567,
685 doi:10.1105/tpc.107.054650 (2008).
686 18 Brzezowski, P. *et al.* The GUN4 protein plays a regulatory role in tetrapyrrole biosynthesis
687 and chloroplast-to-nucleus signalling in *Chlamydomonas reinhardtii*. *Plant J.* **79**, 285-298,
688 doi:10.1111/tpj.12560 (2014).
689 19 Fischer, B. B., Krieger-Liszkay, A. & Eggen, R. I. L. Photosensitizers neutral red (Type I)
690 and rose bengal (Type II) cause light-dependent toxicity in Chlamydomonas reinhardtii and
691 induce the Gpxh gene via increased singlet oxygen formation. *Environ. Sci. Technol.* **38**,
692 6307-6313, doi:10.1021/es049673y (2004).
693 20 Leisinger, U. *et al.* The glutathione peroxidase homologous gene from Chlamydomonas
694 reinhardtii is transcriptionally up-regulated by singlet oxygen. *Plant Mol. Biol.* **46**, 395-408
695 (2001).
696 21 Fischer, B. B., Il Eggen, R. & Niyogi, K. K. Characterization of singlet oxygen-accumulating
697 mutants isolated in a screen for altered oxidative stress response in Chlamydomonas
698 reinhardtii. *BMC Plant Biol.* **10**, doi:279 10.1186/1471-2229-10-279 (2010).
699 22 Fischer, B. B. *et al.* Function and regulation of the glutathione peroxidase homologous gene
700 GPXH/GPX5 in Chlamydomonas reinhardtii. *Plant Mol. Biol.* **71**, 569-583,
701 doi:10.1007/s11103-009-9540-8 (2009).

23 Lunn, J. E. *et al.* Sugar-induced increases in trehalose 6-phosphate are correlated with redox activation of ADPglucose pyrophosphorylase and higher rates of starch synthesis in Arabidopsis thaliana. *Biochem. J.* **397**, 139-148, doi:10.1042/bj20060083 (2006).
24 Yadav, U. P. *et al.* The sucrose-trehalose 6-phosphate (Tre6P) nexus: specificity and mechanisms of sucrose signalling by Tre6P. *J. Exp. Bot.* **65**, 1051-1068, doi:10.1093/jxb/ert457 (2014).
25 Schluepmann, H., Pellny, T., van Dijken, A., Smeekens, S. & Paul, M. Trehalose 6-phosphate is indispensable for carbohydrate utilization and growth in Arabidopsis thaliana. *Proc Natl Acad Sci U S A* **100**, 6849-6854, doi:10.1073/pnas.1132018100 (2003).
26 Fichtner, F. & Lunn, J. E. The Role of Trehalose 6-Phosphate (Tre6P) in Plant Metabolism and Development. *Annu. Rev. Plant Biol.* **72**, 737-760, doi:10.1146/annurev-arplant-050718-095929 (2021).
27 Miller, R. *et al.* Changes in transcript abundance in Chlamydomonas reinhardtii following nitrogen deprivation predict diversion of metabolism. *Plant Physiol.* **154**, 1737-1752, doi:10.1104/pp.110.165159 (2010).
28 Ajalla Aleixo, M. A., Rangel, V. L., Rustiguel, J. K., de Pádua, R. A. P. & Nonato, M. C. Structural, biochemical and biophysical characterization of recombinant human fumarate hydratase. *FEBS J.* **286**, 1925-1940, doi:10.1111/febs.14782 (2019).
29 Yogev, O. *et al.* Fumarase: a mitochondrial metabolic enzyme and a cytosolic/nuclear component of the DNA damage response. *PLoS Biol.* **8**, e1000328, doi:10.1371/journal.pbio.1000328 (2010).
30 Jiang, Y. *et al.* Local generation of fumarate promotes DNA repair through inhibition of histone H3 demethylation. *Nat. Cell Biol.* **17**, 1158-1168, doi:10.1038/ncb3209 (2015).
31 Ma, X. *et al.* Transcriptomic and Physiological Responses to Oxidative Stress in a Chlamydomonas reinhardtii Glutathione Peroxidase Mutant. *Genes* **11**, doi:10.3390/genes11040463 (2020).
32 Blaby, I. K. *et al.* Genome-wide analysis on Chlamydomonas reinhardtii reveals the impact of hydrogen peroxide on protein stress responses and overlap with other stress transcriptomes. *Plant J.* **84**, 974-988, doi:10.1111/tpj.13053 (2015).
33 Urzica, E. I. *et al.* Impact of oxidative stress on ascorbate biosynthesis in Chlamydomonas via regulation of the VTC2 gene encoding a GDP-L-galactose phosphorylase. *J. Biol. Chem.* **287**, 14234-14245, doi:10.1074/jbc.M112.341982 (2012).
34 Roach, T., Stöggl, W., Baur, T. & Kranner, I. Distress and eustress of reactive electrophiles and relevance to light stress acclimation via stimulation of thiol/disulphide-based redox defences. *Free radical biology & medicine* **122**, 65-73, doi:10.1016/j.freeradbiomed.2018.03.030 (2018).
35 Arora, A., Sairam, R. K. & Srivastava, G. C. Oxidative stress and antioxidative system in plants. *Curr. Sci.* **82**, 1227-1238 (2002).
36 Moller, I. M. Plant mitochondria and oxidative stress: Electron transport, NADPH turnover, and metabolism of reactive oxygen species. *Annu. Rev. Plant Physiol. Plant Mol. Biol.* **52**, 561-591 (2001).
37 Asada, K. Production and scavenging of reactive oxygen species in chloroplasts and their functions. *Plant Physiol.* **141**, 391-396, doi:10.1104/pp.106.082040 (2006).
38 Brzezowski, P., Richter, A. S. & Grimm, B. Regulation and function of tetrapyrrole biosynthesis in plants and algae. *Biochimica Et Biophysica Acta-Bioenergetics* **1847**, 968-985, doi:10.1016/j.bbabio.2015.05.007 (2015).
39 Larkin, R. M. Tetrapyrrole Signaling in Plants. *Front. Plant Sci.* **7**, doi:10.3389/fpls.2016.01586 (2016).
40 Moulin, M., McCormac, A. C., Terry, M. J. & Smith, A. G. Tetrapyrrole profiling in Arabidopsis seedlings reveals that retrograde plastid nuclear signaling is not due to Mg-protoporphyrin IX accumulation. *Proc. Natl. Acad. Sci. USA* **105**, 15178-15183, doi:10.1073/pnas.0803054105 (2008).
41 Mochizuki, N., Tanaka, R., Tanaka, A., Masuda, T. & Nagatani, A. The steady-state level of Mg-protoporphyrin IX is not a determinant of plastid-to-nucleus signaling in Arabidopsis. *Proc. Natl. Acad. Sci. USA* **105**, 15184-15189, doi:10.1073/pnas.0803245105 (2008).

42 Vandesteene, L. *et al.* Expansive evolution of the trehalose-6-phosphate phosphatase gene family in Arabidopsis. *Plant Physiol.* **160**, 884-896, doi:10.1104/pp.112.201400 (2012).
43 Ramon, M. *et al.* Extensive expression regulation and lack of heterologous enzymatic activity of the Class II trehalose metabolism proteins from Arabidopsis thaliana. *Plant Cell Environ.* **32**, 1015-1032, doi:10.1111/j.1365-3040.2009.01985.x (2009).
44 Vandesteene, L., Ramon, M., Le Roy, K., Van Dijck, P. & Rolland, F. A single active trehalose-6-P synthase (TPS) and a family of putative regulatory TPS-like proteins in Arabidopsis. *Mol. Plant* **3**, 406-419, doi:10.1093/mp/ssp114 (2010).
45 Delorge, I., Figueroa, C. M., Feil, R., Lunn, J. E. & Van Dijck, P. Trehalose-6-phosphate synthase 1 is not the only active TPS in Arabidopsis thaliana. *Biochem. J.* **466**, 283-290, doi:10.1042/bj20141322 (2015).
46 Collet, J. F., Stroobant, V., Pirard, M., Delpierre, G. & Van Schaftingen, E. A new class of phosphotransferases phosphorylated on an aspartate residue in an amino-terminal DXDX(T/V) motif. *J. Biol. Chem.* **273**, 14107-14112, doi:10.1074/jbc.273.23.14107 (1998).
47 Martins, M. C. *et al.* Feedback inhibition of starch degradation in Arabidopsis leaves mediated by trehalose 6-phosphate. *Plant Physiol.* **163**, 1142-1163, doi:10.1104/pp.113.226787 (2013).
48 Dos Anjos, L. *et al.* Feedback regulation by trehalose 6-phosphate slows down starch mobilization below the rate that would exhaust starch reserves at dawn in Arabidopsis leaves. *Plant direct* **2**, e00078, doi:10.1002/pld3.78 (2018).
49 Zhang, Y. *et al.* Inhibition of SNF1-related protein kinase1 activity and regulation of metabolic pathways by trehalose-6-phosphate. *Plant Physiol.* **149**, 1860-1871, doi:10.1104/pp.108.133934 (2009).
50 Debast, S. *et al.* Altering trehalose-6-phosphate content in transgenic potato tubers affects tuber growth and alters responsiveness to hormones during sprouting. *Plant Physiol.* **156**, 1754-1771, doi:10.1104/pp.111.179903 (2011).
51 Nunes, C. *et al.* Inhibition of SnRK1 by metabolites: tissue-dependent effects and cooperative inhibition by glucose 1-phosphate in combination with trehalose 6-phosphate. *Plant Physiol. Biochem.* **63**, 89-98, doi:10.1016/j.plaphy.2012.11.011 (2013).
52 Zhai, Z. *et al.* Trehalose 6-Phosphate Positively Regulates Fatty Acid Synthesis by Stabilizing WRINKLED1. *Plant Cell* **30**, 2616-2627, doi:10.1105/tpc.18.00521 (2018).
53 Baena-González, E. & Lunn, J. E. SnRK1 and trehalose 6-phosphate - two ancient pathways converge to regulate plant metabolism and growth. *Curr. Opin. Plant Biol.* **55**, 52-59, doi:10.1016/j.pbi.2020.01.010 (2020).
54 Depaepe, T. *et al.* At the Crossroads of Survival and Death: The Reactive Oxygen Species-Ethylene-Sugar Triad and the Unfolded Protein Response. *Trends Plant Sci.* **26**, 338-351, doi:10.1016/j.tplants.2020.12.007 (2021).
55 Baena-González, E., Rolland, F., Thevelein, J. M. & Sheen, J. A central integrator of transcription networks in plant stress and energy signalling. *Nature* **448**, 938-942, doi:10.1038/nature06069 (2007).
56 Gonzalez-Ballester, D., Pollock, S. V., Pootakham, W. & Grossman, A. R. The central role of a SNRK2 kinase in sulfur deprivation responses. *Plant Physiol.* **147**, 216-227, doi:10.1104/pp.108.116137 (2008).
57 González-Ballester, D. *et al.* RNA-seq analysis of sulfur-deprived Chlamydomonas cells reveals aspects of acclimation critical for cell survival. *Plant Cell* **22**, 2058-2084, doi:10.1105/tpc.109.071167 (2010).
58 Colina, F. *et al.* Genome-wide identification and characterization of CKIN/SnRK gene family in Chlamydomonas reinhardtii. *Sci. Rep.* **9**, 350, doi:10.1038/s41598-018-35625-8 (2019).
59 Valledor, L., Furuhashi, T., Hanak, A. M. & Weckwerth, W. Systemic cold stress adaptation of Chlamydomonas reinhardtii. *Mol. Cell. Proteomics* **12**, 2032-2047, doi:10.1074/mcp.M112.026765 (2013).
60 Yang, M., Soga, T., Pollard, P. J. & Adam, J. The emerging role of fumarate as an oncometabolite. *Frontiers in oncology* **2**, 85, doi:10.3389/fonc.2012.00085 (2012).

61 O'Flaherty, L. *et al.* Dysregulation of hypoxia pathways in fumarate hydratase-deficient cells is independent of defective mitochondrial metabolism. *Hum. Mol. Genet.* **19**, 3844-3851, doi:10.1093/hmg/ddq305 (2010).
62 Shanmugasundaram, K. *et al.* The oncometabolite fumarate promotes pseudohypoxia through noncanonical activation of NF-κB signaling. *J. Biol. Chem.* **289**, 24691-24699, doi:10.1074/jbc.M114.568162 (2014).
63 Ternette, N. *et al.* Inhibition of mitochondrial aconitase by succination in fumarate hydratase deficiency. *Cell reports* **3**, 689-700, doi:10.1016/j.celrep.2013.02.013 (2013).
64 Lloyd, S. J., Lauble, H., Prasad, G. S. & Stout, C. D. The mechanism of aconitase: 1.8 A resolution crystal structure of the S642a:citrate complex. *Protein Sci.* **8**, 2655-2662, doi:10.1110/ps.8.12.2655 (1999).
65 Kleine, T., Voigt, C. & Leister, D. Plastid signalling to the nucleus: messengers still lost in the mists? *Trends Genet.* **25**, 185-190, doi:10.1016/j.tig.2009.02.004 (2009).
66 Bräutigam, K. *et al.* Dynamic plastid redox signals integrate gene expression and metabolism to induce distinct metabolic states in photosynthetic acclimation in Arabidopsis. *Plant Cell* **21**, 2715-2732, doi:10.1105/tpc.108.062018 (2009).
67 Pesaresi, P. *et al.* Nuclear photosynthetic gene expression is synergistically modulated by rates of protein synthesis in chloroplasts and mitochondria. *Plant Cell* **18**, 970-991, doi:10.1105/tpc.105.039073 (2006).
68 Shapiguzov, A. *et al.* Arabidopsis RCD1 coordinates chloroplast and mitochondrial functions through interaction with ANAC transcription factors. *eLife* **8**, doi:10.7554/eLife.43284 (2019).
69 Dent, R. M., Haglund, C. M., Chin, B. L., Kobayashi, M. C. & Niyogi, K. K. Functional genomics of eukaryotic photosynthesis using insertional mutagenesis of Chlamydomonas reinhardtii. *Plant Physiol.* **137**, 545-556, doi:10.1104/pp.104.055244 (2005).
70 Depege, N., Bellafiore, S. & Rochaix, J. D. Role of chloroplast protein kinase Stt7 in LHCII phosphorylation and state transition in Chlamydomonas. *Science* **299**, 1572-1575 (2003).
71 Sizova, I., Fuhrmann, M. & Hegemann, P. A Streptomyces rimosus aphVIII gene coding for a new type phosphotransferase provides stable antibiotic resistance to Chlamydomonas reinhardtii. *Gene* **277**, 221-229 (2001).
72 Davies, J. P., Weeks, D. P. & Grossman, A. R. Expression of the arylsulfatase gene from the β2-tubulin promoter in Chlamydomonas reinhardtii. *Nucleic Acids Res.* **20**, 2959-2965 (1992).
73 Schroda, M., Beck, C. F. & Vallon, O. Sequence elements within an HSP70 promoter counteract transcriptional transgene silencing in Chlamydomonas. *Plant J.* **31**, 445-455, doi:10.1046/j.1365-313X.2002.01371.x (2002).
74 Gonzalez-Ballester, D., de Montaigu, A., Galvan, A. & Fernandez, E. Restriction enzyme site-directed amplification PCR: A tool to identify regions flanking a marker DNA. *Anal. Biochem.* **340**, 330-335, doi:10.1016/j.ab.2005.01.031 (2005).
75 Meslet-Cladière, L. & Vallon, O. Novel shuttle markers for nuclear transformation of the green alga Chlamydomonas reinhardtii. *Eukaryot. Cell* **10**, 1670-1678, doi:10.1128/ec.05043-11 (2011).
76 Ohresser, M., Matagne, R. F. & Loppes, R. Expression of the arylsulphatase reporter gene under the control of the nit1 promoter in Chlamydomonas reinhardtii. *Curr. Genet.* **31**, 264-271 (1997).
77 Czarnecki, O., Peter, E. & Grimm, B. in *Chloroplast research in Arabidopsis: Methods and Protocols, Vol II* Vol. 775 357-385 (2011).
78 Figueroa, C. M. *et al.* Trehalose 6-phosphate coordinates organic and amino acid metabolism with carbon availability. *Plant J.* **85**, 410-423, doi:10.1111/tpj.13114 (2016).
79 Fichtner, F. *et al.* Trehalose 6-phosphate is involved in triggering axillary bud outgrowth in garden pea (Pisum sativum L.). *Plant J.* **92**, 611-623, doi:10.1111/tpj.13705 (2017).
80 DuBois, M., Gilles, K. A., Hamilton, J. K., Rebers, P. A. & Smith, F. Colorimetric Method for Determination of Sugars and Related Substances. *Analytical chemistry* **28**, 350-356, doi:10.1021/ac60111a017 (1956).

81 Johnson, X. & Alric, J. Central carbon metabolism and electron transport in Chlamydomonas reinhardtii: metabolic constraints for carbon partitioning between oil and starch. *Eukaryot. Cell* **12**, 776-793, doi:10.1128/ec.00318-12 (2013).
82 Findinier, J. *et al.* The Chlamydomonas mex1 mutant shows impaired starch mobilization without maltose accumulation. *J. Exp. Bot.* **68**, 5177-5189, doi:10.1093/jxb/erx343 (2017).

Acknowledgements

This work was supported by the Deutsche Forschungsgemeinschaft (DFG-GR 936/20-2 to B.G.), by the Agence Nationale de la Recherche (ChloroPaths: ANR-14-CE05-0041-01 to X.J.), and by the Max Planck Society (R.F. and J.E.L.).

Author contributions

P.B. designed the research. P.B. and W.A.Y. performed most of the experiments. R.F. and J.E.L. performed the LC-MS/MS measurements. M.S.-S. and X.J. performed the starch quantification. P.B., B.G., and J.E.L. analysed the data. P.B. wrote the manuscript. P.B., B.G., J.E.L., and X.J. revised the manuscript. All authors discussed the results and commented upon the manuscript.

Competing interests

The authors declare no competing financial interests.

Additional information

Supplementary information accompanies this manuscript:

Supplementary Figure 1. Schematic representation of tetrapyrrole biosynthesis pathway.

Supplementary Figure 2. Schematic representation of the *GPX5-ARS2* reporter gene construct.

Supplementary Figure 3. Analysis of Proto content in *gunSOS1*.

Supplementary Figure 4. Rescue of the $^1O_2$-signalling in *gunSOS1* by introduction of the wild-type *T6PP1*.

Supplementary Figure 5. Metabolites content in *gunSOS1* compared to *sigRep*.

Supplementary Figure 6. Accumulation of fumarate in *gunSOS1* compared to *sigRep* could be explained by increased expression of *FUMARATE HYDRATASE 2*.

Supplementary Figure 7. Accumulation of fumarate in *gunSOS1* compared to *sigRep* could be explained by increased expression of *FUMARYLACETOACETASE*.

898 **Supplementary Figure 8.** Deficiency in aconitate in *gunSOS1* compared to *sigRep* could be
899 explained by decreased expression of *ACONITATE HYDRATASE 1*.
900 **Supplementary Table 1.** Metabolites analyzed in *gunSOS1* compared to *sigRep* (LC-
901 MS/MS).
902 **Supplementary Table 2.** Impact of accumulating metabolites on cell metabolism.
903 **Supplementary Table 3**. Impact of deficient metabolites on cell metabolism.
904 **Supplementary Table 4.** Statistical analyses for $GPX5_{cyt}$ expression following treatment
905 with fumarate, presented in Figure 7a.
906 **Supplementary Table 5.** Statistical analyses for $GPX5_{cp}$ expression following treatment with
907 fumarate, presented in Figure 7a.
908 **Supplementary Table 6.** Statistical analyses for $GPX5_{cyt}$ expression following treatment
909 with aconitate, presented in Figure 7b.
910 **Supplementary Table 7.** Statistical analyses for $GPX5_{cp}$ expression following treatment with
911 aconitate, presented in Figure 7b.
912 **Supplementary Table 8.** Statistical analyses for *SAK1* expression following treatment with
913 aconitate, presented in Figure 7c.
914 **Supplementary Table 9.** Statistical analyses for *PSBP2* expression following treatment with
915 aconitate, presented in Figure 7c.
916 **Supplementary Table 10.** Statistical analyses for *MBS* expression following treatment with
917 aconitate, presented in Figure 7c.
918 **Supplementary Table 11**. Primers used in this study.
919 **Supplementary Data Set 1.** Co-expression analysis
920 **Supplementary Data Set 2.** DEG analysis
921 **Supplementary Data Set 3.** KEGG analysis
922

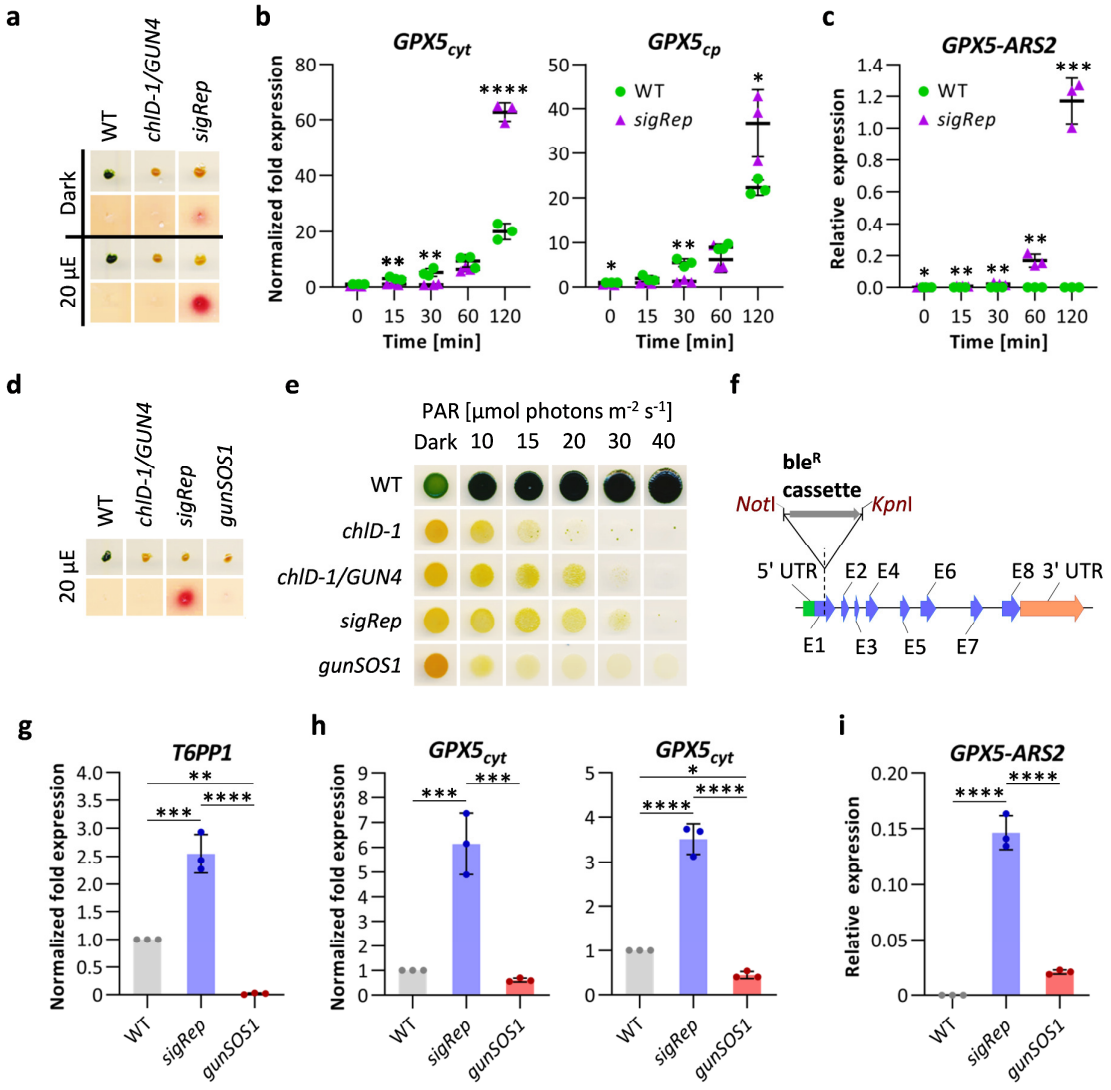
a
WT
chlD-1/GUN4
sigRep
Dark
20 µE
b
GPX5cyt
GPX5cp
Normalized fold expression
Time [min]
WT
sigRep
c
GPX5-ARS2
Relative expression
Time [min]
d
WT
chlD-1/GUN4
sigRep
gunSOS1
20 µE
e
PAR [µmol photons m-2 s-1]
Dark 10 15 20 30 40
WT
chlD-1
chlD-1/GUN4
sigRep
gunSOS1
f
bleR cassette
NotI
KpnI
5' UTR
E2 E4
E6
E8 3' UTR
E1
E3
E5
E7
g
T6PP1
Normalized fold expression
WT
sigRep
gunSOS1
h
GPX5cyt
Normalized fold expression
i
GPX5-ARS2
Relative expression

936 **Figure 1. Generation and initial characterization of the mutant impaired in $^1O_2$-**
937 **signalling. a** Arylsulfatase (ARS2) assay for selection of the strain expressing *GPX5-ARS2*
938 reporter gene in a $^1O_2$-inducible manner. The mutant selected for further applications was
939 named *signalling Reporter* (*sigRep*). WT and *chlD-1/GUN4* do not carry *GPX5-ARS2* and
940 were used as negative controls in ARS2 assay. **b** Expression kinetics of cytosolic ($GPX5_{cyt}$)
941 and chloroplast *GPX5* ($GPX5_{cp}$) in *sigRep* compared to WT upon exposure to light; the
942 values were normalized to WT in dark. **c** Expression of *GPX5-ARS2* in *sigRep* positively
943 correlates with time of exposure to light. WT was used as a negative control. **d** ARS2 activity
944 assay following mutagenesis of *sigRep*. Screen was performed to identify mutants not
945 expressing *GPX5-ARS2* compared to *sigRep* in the same conditions. The mutant selected for
946 further applications was *named genomes uncoupled Singlet Oxygen Signalling 1* (*gunSOS1*).
947 WT and *chlD-1/GUN4* were used as negative controls. **e** Strains with impaired $^1O_2$-signalling
948 demonstrated increased sensitivity to light compared to *sigRep* and *chlD-1/GUN4*. Higher
949 light tolerance of *chlD-1/GUN4* and *sigRep* compared to *chlD-1* is also visible. **f** *T6PP1*
950 (Cre12.g497750) gene model. The insertion (ble^R) was identified in the first exon of 3241 bp
951 *T6PP1*. **g** Expression of *T6PP1* in *gunSOS1* compared to *sigRep*. **h** Expression of $GPX5_{cyt}$
952 and $GPX5_{cp}$ in *gunSOS1* compared to *sigRep*. **i** Expression of *GPX5-ARS2* in *gunSOS1*
953 compared to *sigRep.* WT was used as a negative control. Transcript analyses were performed
954 by qRT-PCR on biological triplicates, values were calculated either as a normalized fold
955 expression ($2^{-\Delta\Delta Ct}$; WT=1) or relative expression ($2^{\Delta Ct}$). For b and c, horizontal bars represent
956 the calculated mean (n = 3), vertical error bars represent calculated ±SD; significant
957 differences were calculated using two-tailed Student's *t*-test and are indicated by asterisks
958 (non-significant not shown), *$P < 0.05$, **$P < 0.01$, ***$P < 0.001$, and ****$P < 0.0001$. For
959 g-i, error bars indicate calculated ±SD; one-way ANOVA, pair-wise comparison with the
960 Tukey's post-hoc test (non-significant not shown), *$P < 0.05$, **$P < 0.01$, ***$P < 0.001$, and
961 ****$P < 0.0001$.
962

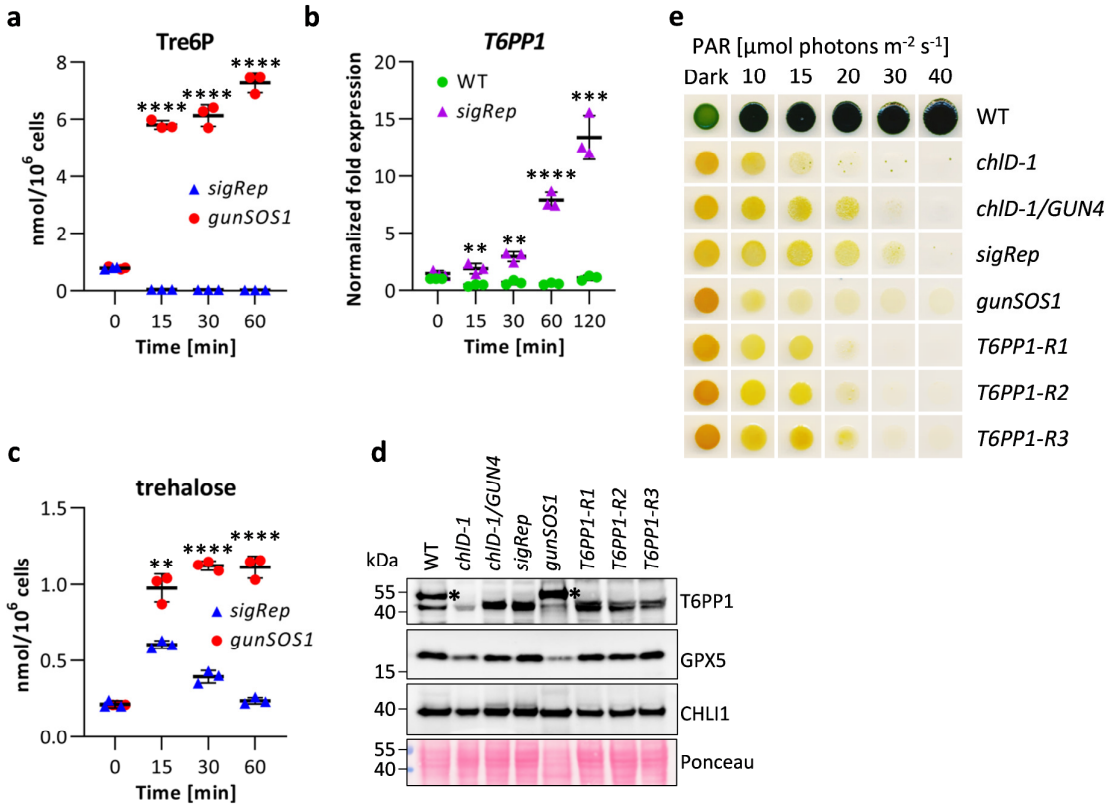

963

964 **Figure 2. *C. reinhardtii* T6PP1 is a functional phosphatase induced during**
965 **photooxidative stress. a** Kinetics of Tre6P accumulation in *gunSOS1* compared to *sigRep*
966 upon transfer from dark to light. **b** Kinetics of *T6PP1* expression upon transfer from dark to
967 light in *gunSOS1* compared to WT indicate inducibility by photooxidative stress rather than
968 light; values were calculated as a normalized fold expression ($2^{-\Delta\Delta Ct}$; WT=1). **c** Higher
969 content of trehalose in *gunSOS1* compared to *sigRep* upon transfer from dark to light may be
970 resulting from the function of T6PS/T6PP1. **d** Immuno-blot analysis of T6PP1 (calculated
971 MW of 42 kDa) and GPX5 content in *gunSOS1* compared to *sigRep* and strains rescued with
972 wild-type copy of *T6PP1*. The CHLI1 content was used as a loading control. The unspecific
973 immunoreaction is indicated by an asterisk. **e** Light sensitivity examination showed that the
974 strains with rescued $^1O_2$-signalling have an increased tolerance to light compared to
975 *gunSOS1*. Experiments in a, b and c were performed in biological triplicates (n = 3)
976 horizontal bars represent the calculated mean, vertical error bars represent ±SD; significant
977 differences were calculated using two-tailed Student's t-test and are indicated by asterisks
978 (non-significant not shown), *$P < 0.05$, **$P < 0.01$, ***$P < 0.001$, and ****$P < 0.0001$.

979

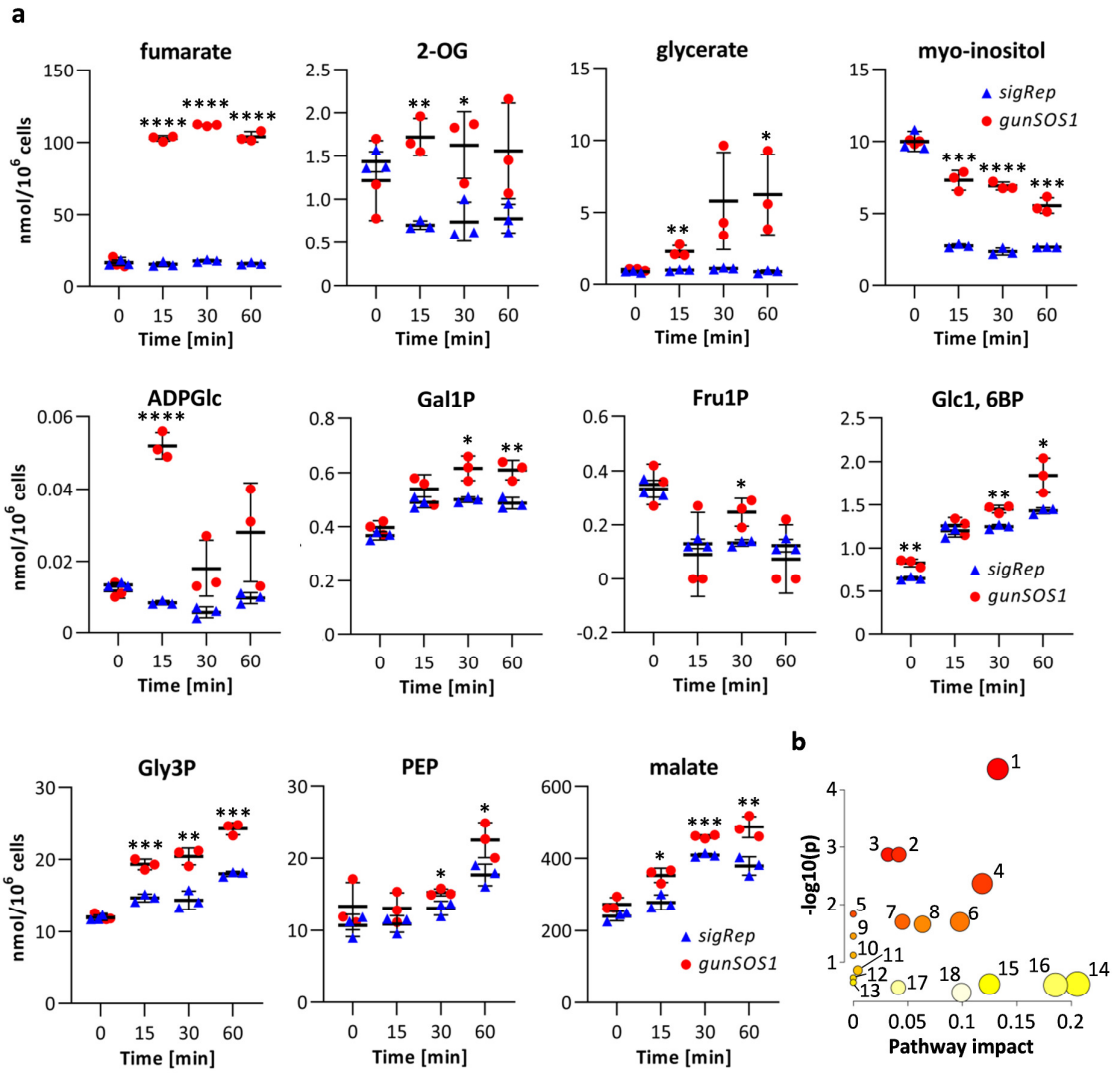
a
fumarate
2-OG
glycerate
myo-inositol
ADPGlc
Gal1P
Fru1P
Glc1, 6BP
Gly3P
PEP
malate
nmol/10^6 cells
Time [min]
sigRep
gunSOS1
b
-log10(p)
Pathway impact

992 **Figure 3. Metabolites with significantly increased content in *gunSOS1* compared to**
993 ***sigRep* in the light. a** LC-MS/MS analysis; fumaric acid (fumarate), oxoglutaric acid (2-OG),
994 myo-Inositol, ADP-glucose (ADPGlc), galactose 1-phosphate (Gal1P), fructose 1-phosphate
995 (Fru1P), alpha-D-Glucose 1,6-bisphosphate (Glc1, 6BP), glycerol 3-phosphate (Gly3P),
996 phosphoenolpyruvic acid (PEP), L-Malic acid (malate). Measurements were performed in
997 biological triplicates and are presented as mean (n = 3), horizontal bars represent the
998 calculated mean, vertical error bars represent calculated ±SD; significant differences were
999 calculated using two-tailed Student's t-test and are indicated by asterisks (non-significant not
1000 shown), *P < 0.05, **P < 0.01, ***P < 0.001, and ****P < 0.0001. **b** Impact of
1001 accumulating metabolites on cell metabolism analysed using MetaboAnalyst 5.0
1002 (https://www.metaboanalyst.ca), sorted by the P value; 1. Tricarboxylic acid cycle (TCA
1003 cycle; P = 4.41E-05), 2. Pyruvate metabolism (P = 0.00136), 3. Starch and sucrose
1004 metabolism (P = 0.00136), 4. Glyoxylate and dicarboxylate metabolism (P = 0.00429), 5.
1005 Arginine biosynthesis (P = 0.01473), 6. Alanine, aspartate and glutamate metabolism (P =
1006 0.02019), 7. Glycerolipid metabolism (P = 0.02019), 8. Carbon fixation in photosynthetic
1007 organisms (P = 0.02217), 9. Galactose metabolism (P = 0.03566), 10. Amino sugar and
1008 nucleotide sugar metabolism (P = 0.07616), 11. Fructose and mannose metabolism (P =
1009 0.13874), 12. Tyrosine metabolism (P = 0.1872), 13. Phenylalanine, tyrosine and tryptophan
1010 biosynthesis (P = 0.22414), 14. Inositol phosphate metabolism (P = 0.24202), 15. Glycolysis
1011 / Gluconeogenesis (P = 0.24202), 16. Phosphatidylinositol signaling system (P = 0.25082),
1012 17. Glycine, serine and threonine metabolism (P = 0.27665), 18. Glycerophospholipid
1013 metabolism (P = 0.34157); detailed results are presented in Supplementary Table 2.
1014

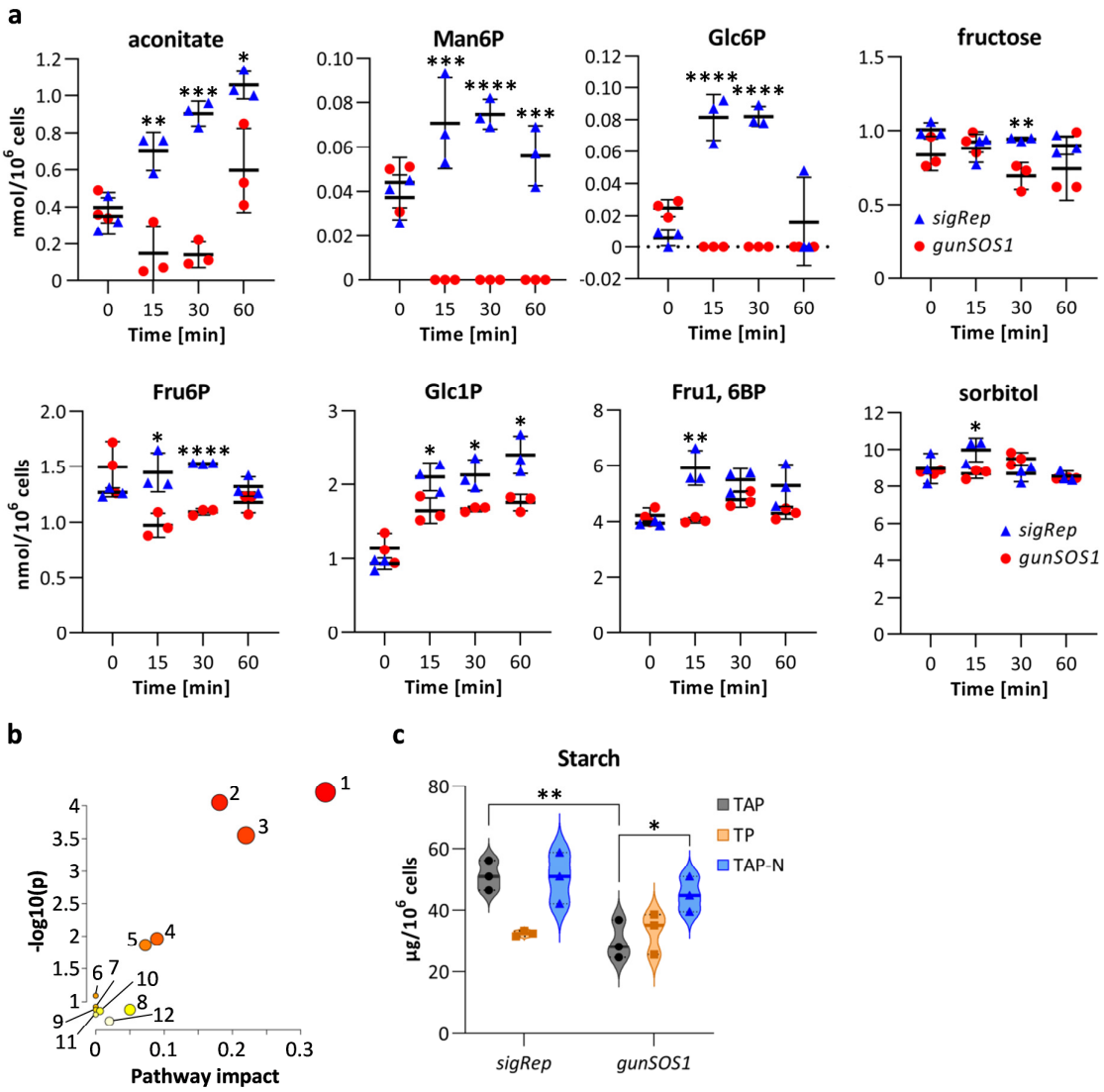
a
aconitate
Man6P
Glc6P
fructose
Fru6P
Glc1P
Fru1, 6BP
sorbitol
nmol/10^6 cells
Time [min]
sigRep
gunSOS1
b
-log10(p)
Pathway impact
c
Starch
µg/10^6 cells
TAP
TP
TAP-N
sigRep
gunSOS1

1027 **Figure 4. Metabolites with significantly decreased content in *gunSOS1* compared to**
1028 ***sigRep* in the light. a** LC-MS/MS analysis; cis-Aconitic acid (aconitate), mannose 6-
1029 phosphate (Man6P), Glucose 6-phosphate (Glc6P), D-fructose (frictose), Fructose 6-
1030 phosphate (Fru6P), Glucose 1-phosphate (Glc1P), Fructose 1,6-bisphosphate (Fru1, 6BP),
1031 sorbitol. Measurements were performed in biological triplicates and are presented as mean (n
1032 = 3), horizontal bars represent the calculated mean, vertical error bars represent calculated
1033 ±SD; significant differences were calculated using two-tailed Student's t-test and are
1034 indicated by asterisks (non-significant not shown), *$P < 0.05$, **$P < 0.01$, ***$P < 0.001$, and
1035 ****$P < 0.0001$. **b** Impact of deficient metabolites on cell metabolism analysed using
1036 MetaboAnalyst 5.0 (https://www.metaboanalyst.ca), sorted by the P value; 1. Fructose and
1037 mannose metabolism (P = 6.23E-05), 2. Amino sugar and nucleotide sugar metabolism (P =
1038 8.99E-05), 3. Starch and sucrose metabolism (P = 0.000282), 4. Glycolysis /
1039 Gluconeogenesis (P = 0.01094), 5. Galactose metabolism (P = 0.013767), 6. Pentose and
1040 glucuronate interconversions (P = 0.081139), 7. Pentose phosphate pathway (P = 0.1195), 8.
1041 Tricarboxylic acid cycle (TCA cycle; P = 0.13197), 9. Glycerolipid metabolism (P =
1042 0.13197), 10. Carbon fixation in photosynthetic organisms (P = 0.13815), 11. Inositol
1043 phosphate metabolism (P = 0.15646), 12. Glyoxylate and dicarboxylate metabolism (P =
1044 0.19785); detailed results are presented in Supplementary Table 3. **c** Starch accumulation in
1045 *gunSOS1* compared to *sigRep.* Measurements were performed in biological triplicates (n = 3);
1046 median is shown as a center line; upper and lower quartiles are shown as dotted lines.
1047 Significant differences were calculated using two-tailed Student's t-test and are indicated by
1048 asterisks (non-significant not shown), *$P < 0.05$, **$P < 0.01$.
1049

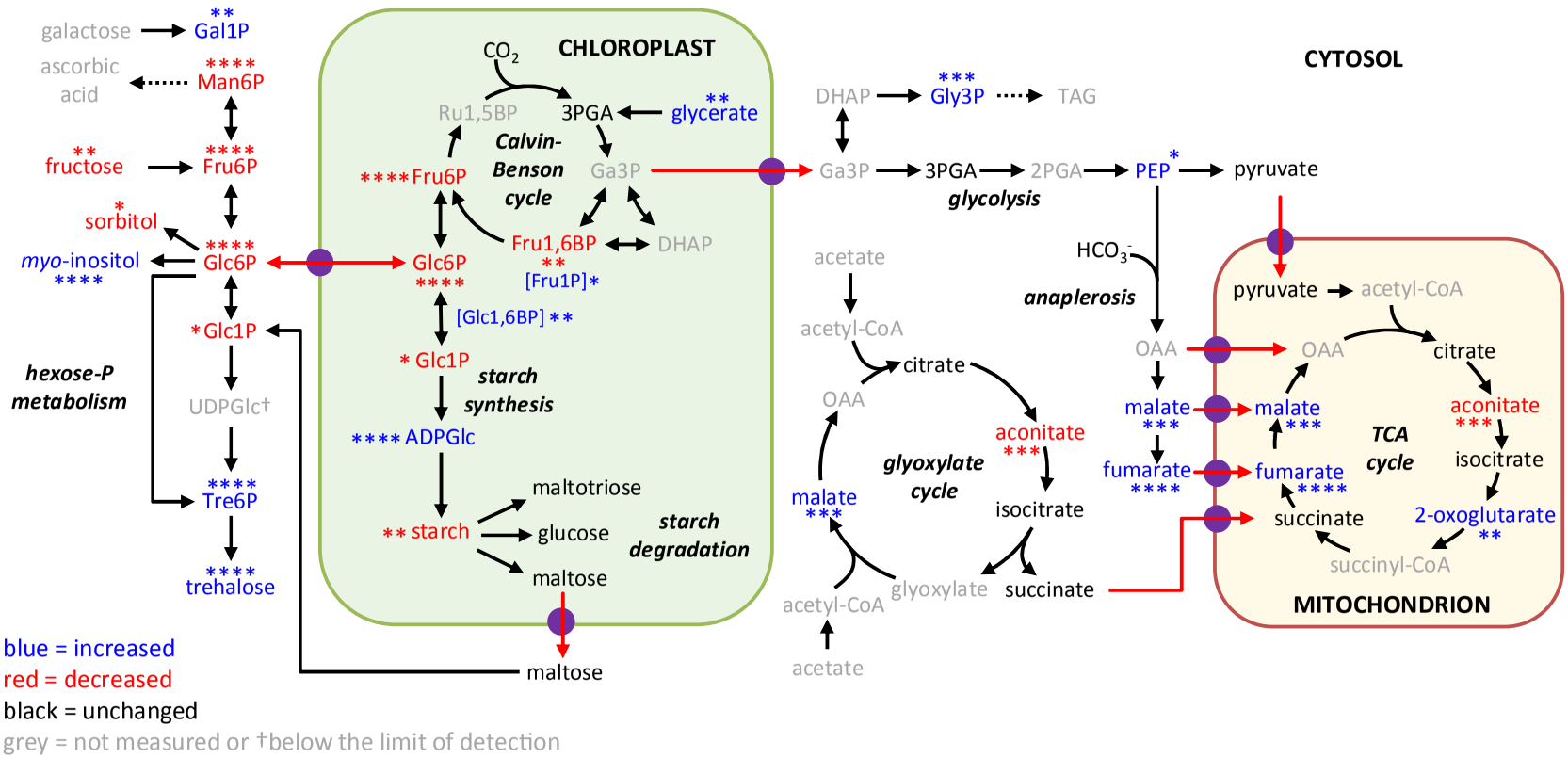
CHLOROPLAST
CYTOSOL
MITOCHONDRION
galactose
Gal1P
ascorbic acid
Man6P
fructose
Fru6P
sorbitol
myo-inositol
Glc6P
Glc1P
UDPGlc†
Tre6P
trehalose
hexose-P metabolism
CO2
Ru1,5BP
3PGA
glycerate
Calvin-Benson cycle
Ga3P
Fru6P
Fru1,6BP
DHAP
[Fru1P]*
Glc6P
[Glc1,6BP]
Glc1P
starch synthesis
ADPGlc
starch
maltotriose
glucose
maltose
starch degradation
maltose
DHAP
Gly3P
TAG
Ga3P
3PGA
2PGA
PEP
pyruvate
glycolysis
HCO3-
anaplerosis
acetate
acetyl-CoA
citrate
OAA
aconitate
isocitrate
malate
glyoxylate cycle
glyoxylate
succinate
acetyl-CoA
acetate
OAA
malate
fumarate
pyruvate
acetyl-CoA
OAA
citrate
malate
aconitate
fumarate
isocitrate
succinate
2-oxoglutarate
succinyl-CoA
TCA cycle
blue = increased
red = decreased
black = unchanged
grey = not measured or †below the limit of detection

1052
1053 **Figure 5. The overview of the selected metabolic pathways in *gunSOS1* compared to**
1054 ***sigRep*.** The map was constructed based on the measured metabolites presented in Figures 3,
1055 4, and Supplementary Figure 5. Metabolites increased in *gunSOS1* compared to *sigRep*:
1056 fumaric acid (fumarate), oxoglutaric acid (2-OG), myo-Inositol, ADP-glucose (ADPGlc),
1057 galactose 1-phosphate (Gal1P), fructose 1-phosphate (Fru1P), alpha-D-Glucose 1,6-
1058 bisphosphate (Glc1, 6BP), glycerol 3-phosphate (Gly3P), phosphoenolpyruvic acid (PEP), L-
1059 Malic acid (malate). Metabolites decreased in *gunSOS1* compared to *sigRep*: cis-Aconitic
1060 acid (aconitate), mannose 6-phosphate (Man6P), Glucose 6-phosphate (Glc6P), D-fructose
1061 (frictose), Fructose 6-phosphate (Fru6P), Glucose 1-phosphate (Glc1P), Fructose 1,6-
1062 bisphosphate (Fru1, 6BP), and sorbitol. Metabolites that did not show significant difference
1063 in gunSOS1 relative to sigRep: D-Glucose (glucose), D-Maltose (maltose), maltotriose, citric
1064 acid (citrate), isocitric acid (isocitrate), pyruvic acid (pyruvate), succinic acid (succinate), 3-
1065 phosphoglyceric acid (3PGA). The colour-coding: blue = increased, red = decreased, black =
1066 unchanged, grey = not measured or [a]below the limit of detection. Significant differences were
1067 calculated using two-tailed Student's *t*-test. The maximal significant differences from any
1068 time point in light (Fig. 4 and 5) are indicated by asterisks, $*P < 0.05$, $**P < 0.01$, $***P <$
1069 0.001, and $****P < 0.0001$. The metabolic map was constructed based on the review by[81]
1070 and[82].
1071
1072

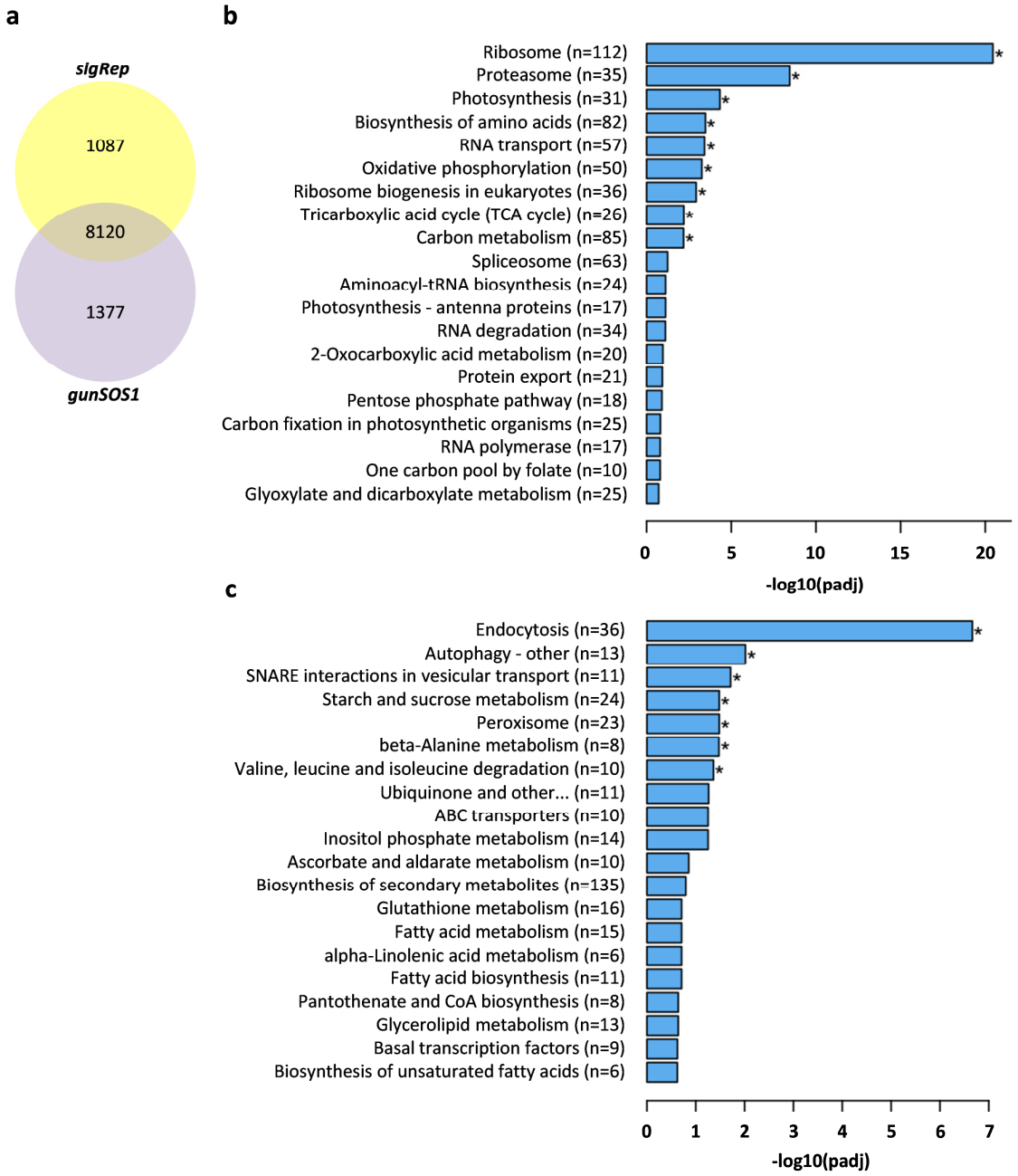

Figure 6. Transcriptome analysis based on RNA-seq. a Venn diagram showing number of genes expressed in *gunSOS1* and *sigRep* (8120), or uniquely expressed in *gunSOS1* (1377) or in *sigRep* (1087). **b** Pathway enrichment analysis (KEGG, http://www.kegg.jp/) based on the differentially expressed genes (RNA-seq); genes down-regulated in *gunSOS1* compared to *sigRep*. **c** KEGG analysis showing genes up-regulated in *gunSOS1* compared to *sigRep*. Effect on metabolic processes is sorted by the *p* value. Asterisk indicates the core (significant) enrichment.

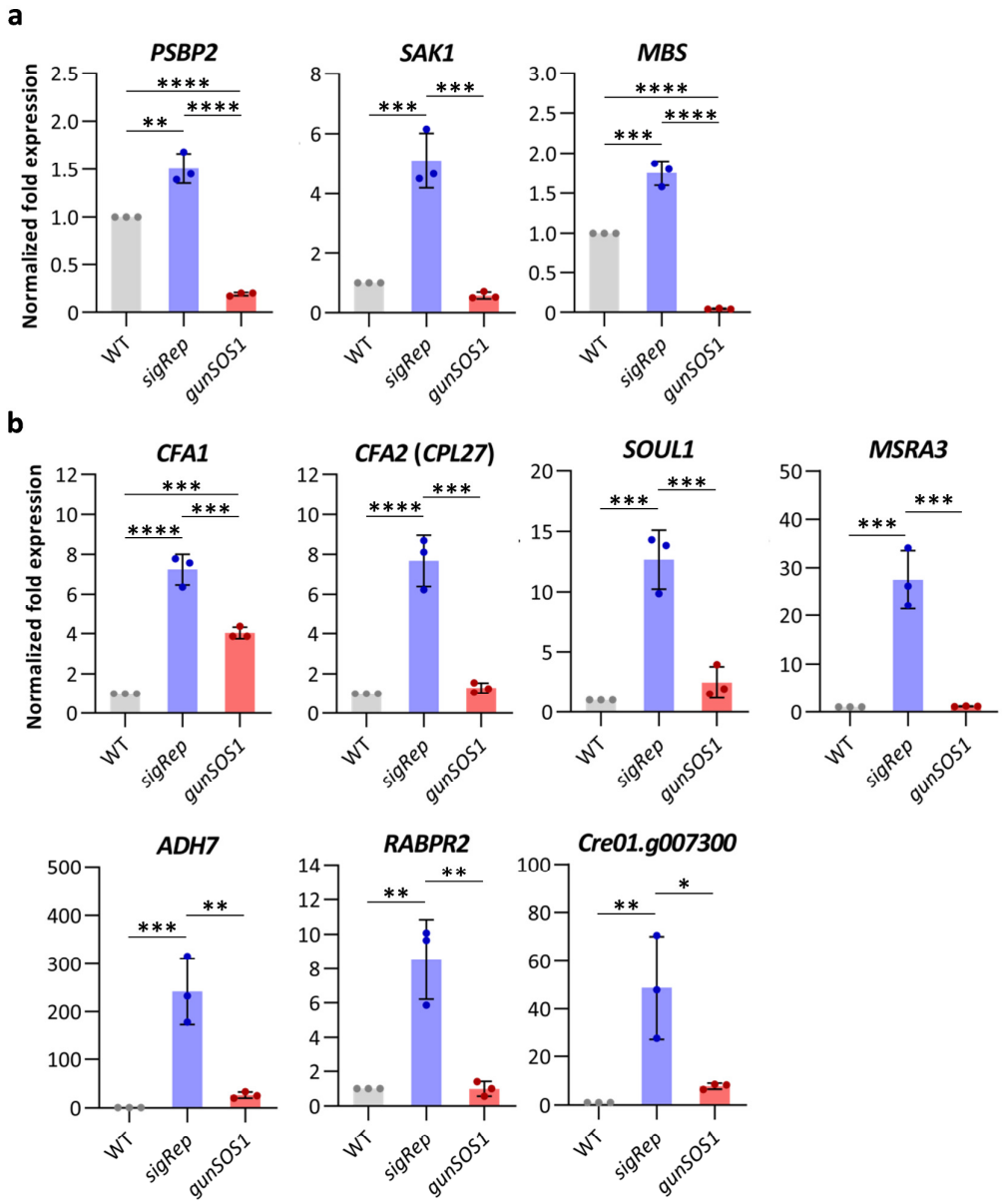

1082
1083 **Figure 7. The qRT-PCR analysis of gene expression in *gunSOS1* compared to *sigRep*. a**
1084 Expression of genes encoding proteinaceous components previously associated with the
1085 chloroplast retrograde signalling involving $^1O_2$, *PSBP2*[14], *SAK1*[15], and *MBS*[16]. **b** transcript
1086 levels of the selected genes showing attenuated expression in *gunSOS1* compared to *sigRep*
1087 in the context of the SAK1-transcriptome[15], genes description in the text. Experiments were
1088 performed in biological replications; results are presented as normalized fold expression (2^{-}
1089 $^{\Delta\Delta Ct}$, WT=1); the error bars represent calculated ±SD. Significant differences were calculated
1090 using one-way ANOVA, pair-wise comparison with the Tukey's post-hoc test (non-
1091 significant not shown), *$P < 0.05$, **$P < 0.01$, ***$P < 0.001$, and ****$P < 0.0001$.

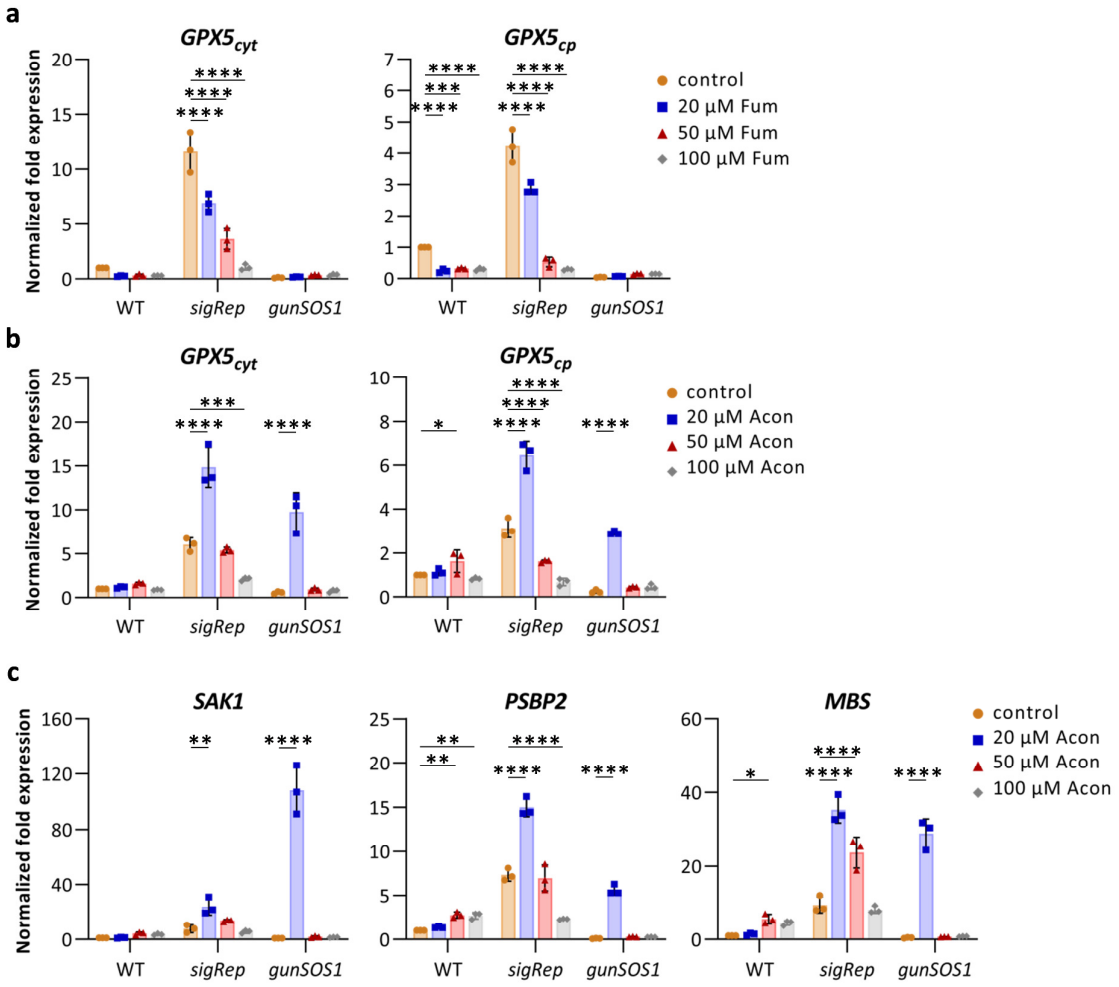
a
GPX5cyt
GPX5cp
Normalized fold expression
control
20 µM Fum
50 µM Fum
100 µM Fum
WT
sigRep
gunSOS1
b
GPX5cyt
GPX5cp
Normalized fold expression
control
20 µM Acon
50 µM Acon
100 µM Acon
WT
sigRep
gunSOS1
c
SAK1
PSBP2
MBS
Normalized fold expression
control
20 µM Acon
50 µM Acon
100 µM Acon
WT
sigRep
gunSOS1

1113 **Figure 8. Effect of selected metabolites applied exogenously on $^1O_2$-signalling inducing**
1114 ***GPX5$_{cyt}$ or GPX5$_{cp}$* expression. a** Fumarate (Fum) significantly (P < 0.0001) decreased
1115 *GPX5* expression in *sigRep* in concentration-dependent manner. Interaction between mutants
1116 and fumarate, as well as the mutant-dependent expression of *GPX5* were also significant, P <
1117 0.0001 and P < 0.001, respectively. Fumarate had no effect on *GPX5$_{cyt}$* expression in
1118 *gunSOS1* or WT, but attenuating effect was observed for *GPX5$_{cp}$* expression in WT ($P \leq$
1119 0.0001). Detailed reports from statistical analyses are presented in Supplementary Tables 4
1120 and 5. **b** Aconitate (Acon) at 20 µM concentration rescues *GPX5* expression in *gunSOS1* and
1121 increases *GPX5* expression in *sigRep*. Statistical analysis showed that 20 µM aconitate
1122 significantly ($P \leq 0.0001$) affect *GPX5$_{cyt}$* expression in *gunSOS1* and *sigRep*, but 100 µM
1123 concentration (P = 0.0001) decreased this expression in *sigRep*. An increase in *GPX5$_{cp}$*
1124 expression (P < 0.05) was also observed in WT upon treatment with 50 µM aconitate
1125 (Supplementary Table 6 and 7). **c** Transcripts content for proteins necessary for the $^1O_2$-
1126 signalling, *SAK1*, *PSBP2*, and *MBS* significantly (P < 0.01) increased upon treatment with 20
1127 µM aconitate. An increase in *PSBP2* and *MBS* expression was also observed in WT treated
1128 with 50 µM aconitate. Detailed statistical analyses are presented in Supplementary Tables 8-
1129 10. The qRT-PCR experiments were performed in biological replications (n = 3); results are
1130 presented as normalized fold expression ($2^{-\Delta\Delta Ct}$, untreated WT=1); the error bars represent
1131 calculated ±SD. Significant differences were calculated using two-way ANOVA with
1132 Dunnett's multiple comparison test and are indicated by asterisks (non-significant changes
1133 are not shown on the graph for clarity), *P < 0.05, **P < 0.01, ***P < 0.001, and ****P <
1134 0.0001.
1135
1136

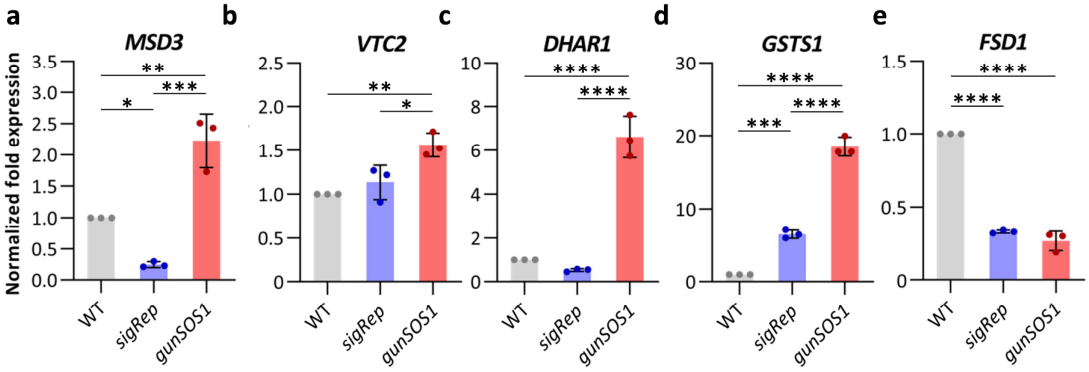

Figure 9. Expression of genes, which induction was previously associated with H_2O_2 or organic peroxides, but not with $^1O_2$. a *Mn superoxide dismutase 3* (*MSD3*). **b** *ASCORBATE PEROXIDASE 1* (*APX1*). **c** *Mono-functional catalase* (*CAT1*). **d** *GDP-L-galactose Phosphorylase* (*VTC2*). **e** *monodehydroascorbate reductase* (*MDAR1*). **f** *dehydrosascorbate reductase* (*DHAR1*) **g** *GLUTATHIONE REDUCTASE* (*GSHR1*). **h** *γ-glutamylcysteine synthetase* (*GSH1*). **i** *Glutathione S-transferase* (*GSTS1*). **j** *Fe superoxide dismutase* (*FSD1*). Experiments were performed in biological replications (n = 3); results are presented as normalized fold expression ($2^{-\Delta\Delta Ct}$, WT=1); the error bars represent calculated ±SD. Significant differences were calculated using one-way ANOVA, pair-wise comparison with the Tukey's post-hoc test (non-significant not shown), *$P < 0.05$, **$P < 0.01$, ***$P < 0.001$, and ****$P < 0.0001$.

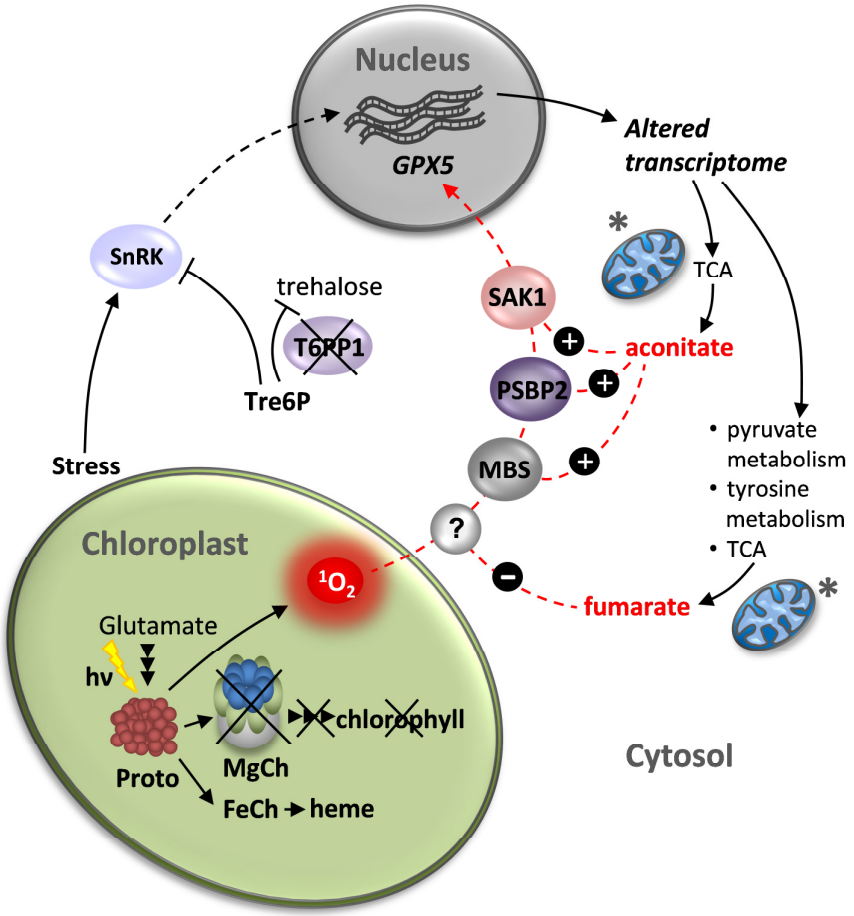

Figure 10. Model of the chloroplast $^1O_2$-induced retrograde signalling depending on the metabolite content. Lack of functional Mg-chelatase (MgCh) leads to accumulation of protoporphyrin IX (Proto), which in light generates $^1O_2$. Lack of functional T6PP1 results in accumulation of trehalose 6-phosphate (Tre6P), which inhibits SnRK. Blocked SnRK signalling pathway leads to the inadequate transcriptomic response to stress and disturbed metabolites content. Fumarate accumulated due to the altered expression of genes involved in pyruvate metabolism, tyrosine metabolism and the TCA cycle. Accumulation of fumarate and disturbed TCA cycle lead to deficiency in aconitate. Fumarate attenuate $^1O_2$-signalling through yet unknown factor (marked with a question mark). The proteinaceous components, PSBP2, MBS, and SAK1, previously demonstrated to be required for $^1O_2$-signalling are shown. Aconitate is promoting expression of *PSBP2*, *MBS*, and *SAK1* in *gunSOS1* mutant. Mitochondria are marked by an asterisk.